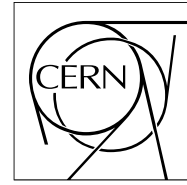


The Compact Muon Solenoid Experiment
Analysis Note



The content of this note is intended for CMS internal use and distribution only

25 July 2008

Neutral Pion rejection for isolated and unconverted photon candidates using CMS ECAL and Preshower detector

K. Karafasoulis, A. Kyriakis

INP, NCSR DEMOKRITOS, Agia Paraskevi, Athens 15310, GREECE

D. Maletic

INS VINCA, Belgrade, Serbia

Abstract

Applying a general Artificial Neural Network approach, the possibility to discriminate neutral pions (π^0) from photons was studied using information from both ECAL and Preshower subdetectors. For unconverted particles the obtained neutral pion rejection could vary between 29% and 76% depending on the method used for selecting unconverted particles, the transverse energy and the pseudorapidity. The test of the algorithm on $H \rightarrow \gamma\gamma$ and $\gamma + \text{Jet}$ events showed that, in case of both photons are unconverted, the $\gamma + \text{Jet}$ background could be reduced by 46% to 57% maintaining almost 85% to 88% of the Higgs events respectively and this depends on the choice of the unconversion method used.

1 Introduction

A significant background to the $H \rightarrow \gamma\gamma$ process originates from π^0 's in jets, which fake single isolated photons. Thus, an electromagnetic cluster may be due to an incident photon, or a pair of closely-spaced photons from the decay of a π^0 inside a jet. The lateral shape of the energy deposit in the Electromagnetic calorimeter (ECAL) can be used to distinguish a π^0 from a photon especially at low energies where the separation between the photons from the π^0 decay is large.

For the ECAL barrel a method developed for L3 [1] was adapted and it is based on analysis of the patterns of energy deposited in the ECAL by electromagnetically showering particles. In this note these patterns are referred as *shower shapes*. A shower shape analysis consist of examining the response of the electromagnetic calorimeter, and can yield information about the type of particle (or particles) responsible for the observed energy deposits.

In about half of the $H \rightarrow \gamma\gamma$ decays at least one of the photons will fall in the rapidity interval covered by the endcaps. In this region, the π^0 's have higher energies than in the barrel and decay into two closely-spaced (of the order of a few mm) photons, which are indistinguishable from single photons using only the information taken from the ECAL crystals.

The endcap preshower, a position-sensitive device with high granularity, is placed in front of the endcap ECAL crystals. A full description of the preshower can be found elsewhere [2]. The fine granularity of the preshower detector can be used to distinguish energy deposits due to double-photons from π^0 's from those due to single photons giving a significant boost to $\gamma - \pi^0$ separation.

In this note we present the results of a study of the π^0 rejection in both the ECAL barrel and endcap regions using combined ECAL and preshower information under an Artificial Neural Net (ANN) approach.

In the following sections, we first give a general description of a ANN, then we describe the input variables used in both the barrel and endcap ANN implementation. The note follows with the description of the performance of a ANN for different particles' transverse momentum. Finally, we use this algorithm on $H \rightarrow \gamma\gamma$ signal events and $\gamma + \text{Jet}$ background events.

2 General description of an ANN

The first attempts for the construction of an ANN were motivated by the desire to create models of the human brain. Much later, it was discovered that ANN's are a very general statistical framework for modelling posterior probabilities, given a set of input data.

The basic building block of an ANN is the 'neuron'. A neuron is a processing unit, having several inputs and at least one output. Generally the ANN's are built by arranging groups of neurons into layers and connecting the outputs of the neurons from one layer to the inputs of the neurons of the next layer.

The first layer is called the *input* layer because the discriminating variables are fed to it. There should be one neuron per input variable. The input layer is followed by a number of internal, so called *hidden* layers and finally there is the *output* layer. A typical topology of ANN can be seen in figure 1

There are many types of ANN, but one of the most favored in terms of pattern recognition problems is the 'feed-forward backpropagation ANN' [3]. We used a three layer ANN (fig. 1) with only one hidden layer, which is the most common architecture for pattern recognition problems.

The ANN operates in three phases :

- **Supervised learning** : events belonging to each class (in our case the two classes are for single photons and double-photons from π^0 s) are presented to the system in order to train it to recognize their features. The output O_i of each neuron i is obtained by applying a transition function, the so-called 'activation function' on the weighted sum of its inputs j , which are the outputs of the neurons of the previous layer O_j :

$$O_i = f(W_{i0} + \sum_{j=1}^N W_{ij}O_j)$$

where : W_{ij} are the connection weights between neurons i , of layer l and j , of layer $l - 1$, W_{i0} is the

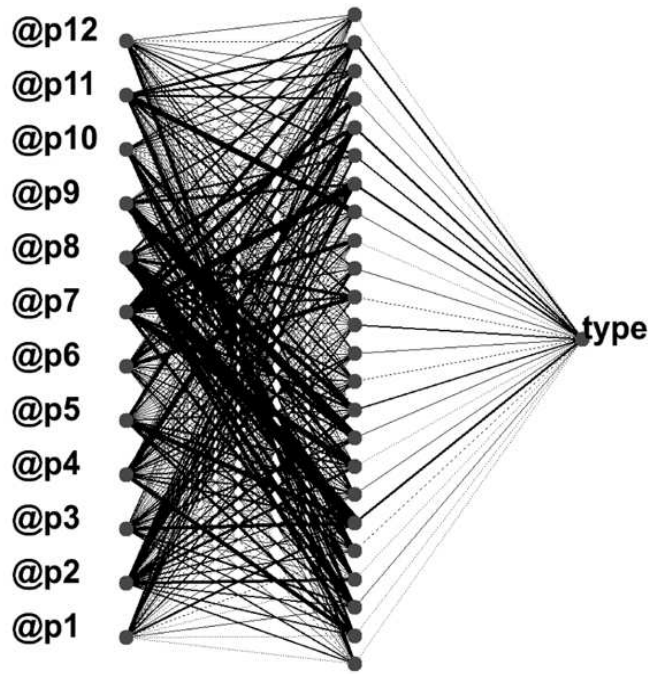


Figure 1: A typical topology of an ANN with 12 input nodes, 24 hidden nodes and 1 output node.

threshold of neuron i , N is the number of the input variables and

$$f(x) = \frac{1}{1 + e^{-cx}}$$

is the logistic activation function, which is a sigmoidal or ‘S-shape’ curve.

The weights are determined by using the gradient descent method in an iterative procedure, where several passes through the set of the events are used to optimize the weights. At each step the weights $W_{ij}(t + 1)$ depend on the weights from the previous step $W_{ij}(t)$ and are changed as :

$$W_{ij}(t + 1) = W_{ij}(t) + \Delta W_{ij}(t + 1)$$

$$\Delta W_{ij}(t + 1) = -\eta \frac{\partial E}{\partial W_{ij}} + \alpha \Delta W_{ij}(t)$$

where: η is the learning factor (a constant usually between 0.1 and 1.), α is the momentum term which introduces the old weight change as a parameter for the computation of the new weight change (a constant usually between 0.1 and 1.) and E is the sum-of-squares error for the specific learning step, defined as :

$$E = \sum_{k=1}^{N_{events}} (O_k - T_k)^2$$

where : O_k is the ANN output for set k and T_k is the corresponding true value (0 = background, 1 = signal) and N_{events} is the total number of events.

- **Validation step** : when the learning phase is finished a second, ‘unknown’, sample of events is presented to the ANN to test the ability of the net to recognize events it has never seen before.
- **Real test** : after the net has proven its generalization it is tested on ‘real’ events.

3 Event selection

In this analysis three data sets were used, all produced under the CSA07 [4] official production schedule without pileups and with the $100pb^{-1}$ misalignment and miscalibration scenario:

- a set of $\gamma + \text{Jet}$ events with isolated π^0 s inside the jet forced from the generated level and with various π^0 s E_T ranges: 15-25,25-35,35-45,45-55,55-65 GeV called from now on "GammaJetIsoPi0" events.
- $H \rightarrow \gamma\gamma$ events with Higgs mass of $120GeV/c^2$ called from now on "Official Higgs" events
- $\gamma + \text{Jet}$ events from now on called "Official GammaJet" events

The first set of events was mainly used to train the ANN and calculate the efficiency of the algorithm while the next two were used for testing with more realistic events.

In all the events we first applied "HLT2Photon" trigger. According to a reference [5] this trigger is based on isolated L1 trigger ECAL objects with a p_T threshold of $p_T > 20GeV/c$ for both photons and has a rate of $0.6 \pm 0.4 \text{ Hz}$ at $L = 10^{32}cms^{-2}s^{-1}$.

3.1 Isolation Condition

After HLT application strong isolation criteria for the photons and π^0 s based on tracker information only were applied. In fact photons or π^0 s were considered to be isolated if the p_T sum of the tracks with $p_T > 1.5GeV/c$ in a cone of $dR = \sqrt{d\eta^2 + d\phi^2} < 0.3$ around the photon's or π^0 's direction over the particle's E_T measured by ECAL was less than 0.01. In figure 2 is shown the isolation of photons coming from $H \rightarrow \gamma\gamma$ events and π^0 from "Official GammaJet" events.

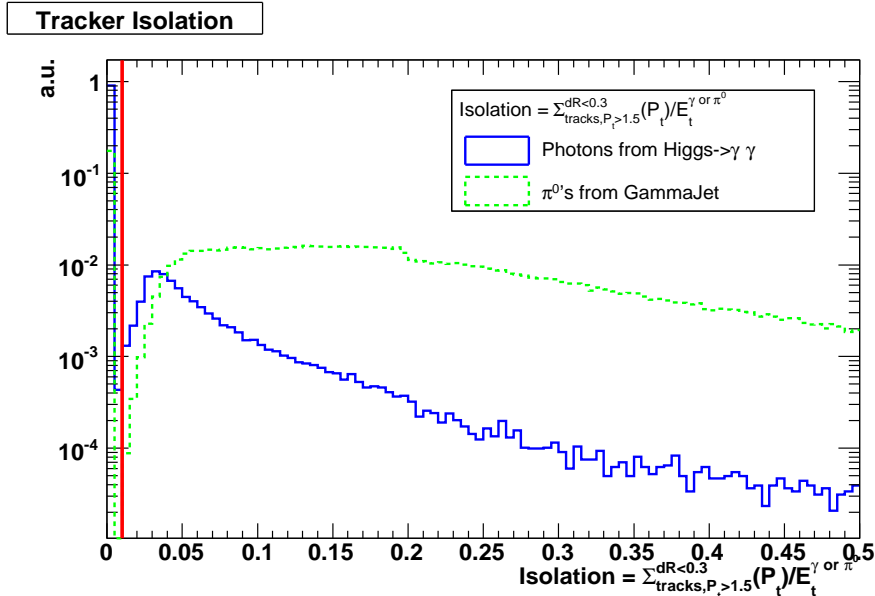


Figure 2: Isolation for photons coming from $H \rightarrow \gamma\gamma$ events and π^0 s from "Official GammaJet" events. The isolation is defined as a ratio of the p_T sum of the tracks with $p_T > 1.5GeV/c$ in a cone of $dR = \sqrt{d\eta^2 + d\phi^2} < 0.3$ around the photon's or π^0 's direction over the particle's E_T measured by ECAL. The vertical line shows the cut of 0.01 that has been set.

3.2 Selection of unconverted particles

After the application of isolation we restricted ourselves to unconverted photons or π^0 . This selection is done by using two available methods.

- The first method is based on R9 cut called the "R9 > 0.93" method. R9 is the ratio of energy sum deposited in a 3×3 ECAL crystal matrix around the crystal of maximum energy (S_1) over the energy of the ECAL super cluster. We defined as unconverted particles the ones with $R9 > 0.93$, used the same way as in [6].

- The second method is the "track finding for identification of converted photons" method called " $N_{trk}^{ConvID} = 0$ " method, described in details in [7]. In principle, the e^-/e^+ tracks that come from photon conversions at large radii can not be identified by the standard tracking algorithm that uses pixel detector hits as seeds. So the " $N_{trk}^{ConvID} = 0$ " method starts from an ECAL super cluster and takes into account the magnetic field and the vertex information. The method takes into account also the fact that conversions mainly happen in the material of the inner tracker, so it tries to find associated hits in the inner tracker only. If this is the case, this method uses these hits as a seed for a track finding procedure. Obviously, this method does not work for late converted photons that convert in a radius of $R > 85cm$ in the barrel or $Z > 210cm$ in the endcaps. Finally, by using this method we define a photon or a π^0 to be unconverted when a super cluster is not associated with a track.

In summary, the analysis was based on the "HTL2Photon" trigger selection followed by the isolation criteria and the unconverted particle criteria as defined above.

4 ANN input variables

For the Neural Network analysis, we used the JETNET 3.5 package [8]. The topology of the Neural Net was 12 - 24 - 1 for the barrel (Figure 1) and 25 - 26 - 1 (25 nodes in the input layer, 26 nodes in the hidden layer and 1 node as output) for the ECAL endcap.

We chose the 'back-propagation' algorithm with *fixed momentum term* of $\alpha = 0.1$ and a *running learning factor*. The activation function was the *logistic* and the error function was the *sum-of-squares error* function [9].

4.1 Barrel region - Shower shape variables

A *shower shape variable* is a quantity that is derived from the crystals' energies in a cluster and that is sensitive to differences between single and overlapping photon showers[10]. The electromagnetic shower generated by a single unconverted photon is approximately axially symmetric about the incident photon's direction. When the shower from two photons overlap, their combined energy deposit is a superposition of the energy deposits of individual photons, with an offset between them. The resulting shower shape is no longer axially symmetric and thus it can, in principle, be distinguished from the shower shape of a single photon. The general strategy for choosing shower shape variables is therefore to identify quantities that measure the "roundness" of the energy deposition in a cluster. However, quantifying this roundness can be technically difficult, because the angular segmentation of the ECAL is coarse with respect to the characteristic transverse size of a shower. As a result, geometric effect can obscure the roundness of the shower from a single photon when it is incident near the edge of a crystal.

A simple and effective class of shower-shape variables consists of ratios of crystals' energy sums, $S_{inner}/(S_{inner} + S_{outer})$, which measure how much of the total energy deposited in a region is concentrated in an inner central region. These ratios are typically larger for single-photon showers than for multiple-overlapping-photon showers, and are reasonably insensitive to geometrical effects since they use crystal-energy sums rather than individual crystal energies. The following nine shower-shape variables based on energy ratios were selected;

$$p_6 = \frac{S_4}{S_{25}}, p_4 = \frac{S_1}{S_9}, p_5 = \frac{S_9 - S_1}{S_{25} - S_1}$$

$$p_{12} = \frac{M_2 + S_1}{S_4}, p_9 = \frac{S_6}{S_9}, p_{11} = \frac{M_2 + S_1}{S_9}, p_8 = S_{6-ratio}$$

$$p_1 = |x_{cog}|_{25} = \left| \frac{\sum_{i=1}^{25} E_i X_i^{rel}}{S_{25}} \right|, p_7 = |y_{cog}|_{25} = \left| \frac{\sum_{i=1}^{25} E_i Y_i^{rel}}{S_{25}} \right|$$

where S_1 is the largest and M_2 the second largest crystal energy in a cluster, S_9 (S_{25}) is the sum of energies for the surrounding 3×3 (5×5) matrix of crystals around S_1 , and S_4 is the largest of the four possible 2×2 crystal energy sums that include the first (S_1) most energetic crystal. The S_6 is defined as the largest of the four possible 2×3 crystal energy sums that include the first (S_1) and the second (M_2) most energetic crystal as can be seen in figure 3. The S_6 and $S_{6-ratio}$, also seen in figure 3, are non zero only if the M_2 is one of the closest 4 crystals to S_1 (forming a Greek cross around S_1). The $S_{6-ratio}$ is the ratio which numerator is a sum of energies of two

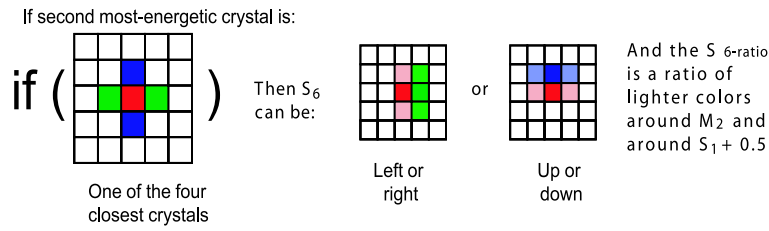


Figure 3: The definition of S_6 and $S_{6-ratio}$

closest crystals - none of them S_1 - positioned left and right (up and down) from M_2 , forming a line with M_2 . $S_{6-ratio}$'s denominator is the sum of energies of two closest crystals - none of them M_2 - positioned left and right (up and down) from the S_1 , forming a line with S_1 , with addition of a value 0.5 to denominator to avoid division by zero. The X_i^{rel} and Y_i^{rel} are coordinates relative to S_1 .

A second class of shower-shape variables is based on a moment analysis of the crystal energies in a 5×5 matrix, $E_{\eta\phi}$, where η and ϕ are the position coordinates of a cluster. There is a need to calculate log weight [11] of each crystal w_c , sum of log weights $\sum_{c=1}^{25} w_c$ and covariances, $\sigma_{i,j}$, and then to define two variables corresponding to the distribution of log weights of the crystal energy in the η and ϕ projections

$$\sigma_{xy} = \frac{\sum_{c=1}^{25} (x^c - \langle x \rangle)(y^c - \langle y \rangle)w_c}{\sum_{c=1}^{25} w_c}$$

where x and y correspond to η or ϕ and

$$w_c = MAX(0., w_0 + \log(E_c/S_{25}))$$

$$p_2 = \frac{\sigma_{\eta\eta}}{0.0004}, p_3 = \frac{\sigma_{\phi\phi}}{0.001}$$

The eigenvalues of the covariance matrix can be also calculated:

$$\lambda_{\pm} = \frac{\sigma_{\eta\eta} + \sigma_{\phi\phi} \pm \sqrt{(\sigma_{\eta\eta} - \sigma_{\phi\phi})^2 + 4\sigma_{\eta\phi}^2}}{2}$$

which are related to the lengths of the principal axes of the distribution of log weights of the crystal energy, and then define

$$p_{10} = \frac{\lambda_-}{\lambda_+}$$

which measures the eccentricity of the distribution of log weights of the crystal energy.

Figure 4 shows a distribution of input variables for the ECAL Barrel created by the "GammaJetIsoPi0" sample with unconverted(using " $N_{trk}^{ConvID} = 0$ " method) particles of E_T of 20 GeV (figure 4 a) and E_T of 60 GeV (figure 4 b). The corresponding plot for unconverted(using " $R9 > 0.93$ " method) particles is shown in figure 5. Clearly some variables like $c_{\eta\eta}/0.0004$ or s_4/s_{25} seems to discriminate better the two samples when the " $R9 > 0.93$ " method is used to select unconverted particles especially in lower E_t . This fact will influence the separation power as will be seen in section 5.

Figure 6 shows indicatively the linear correlations of input variables for unconverted(using " $N_{trk}^{ConvID} = 0$ " method) signal (photon) and background (π^0) of E_T 20GeV[12].

4.2 Preshower endcap region

A detailed description of the method used for the Preshower endcap region can be found in a reference [13] and can be shown in figure 7 (a). So briefly:

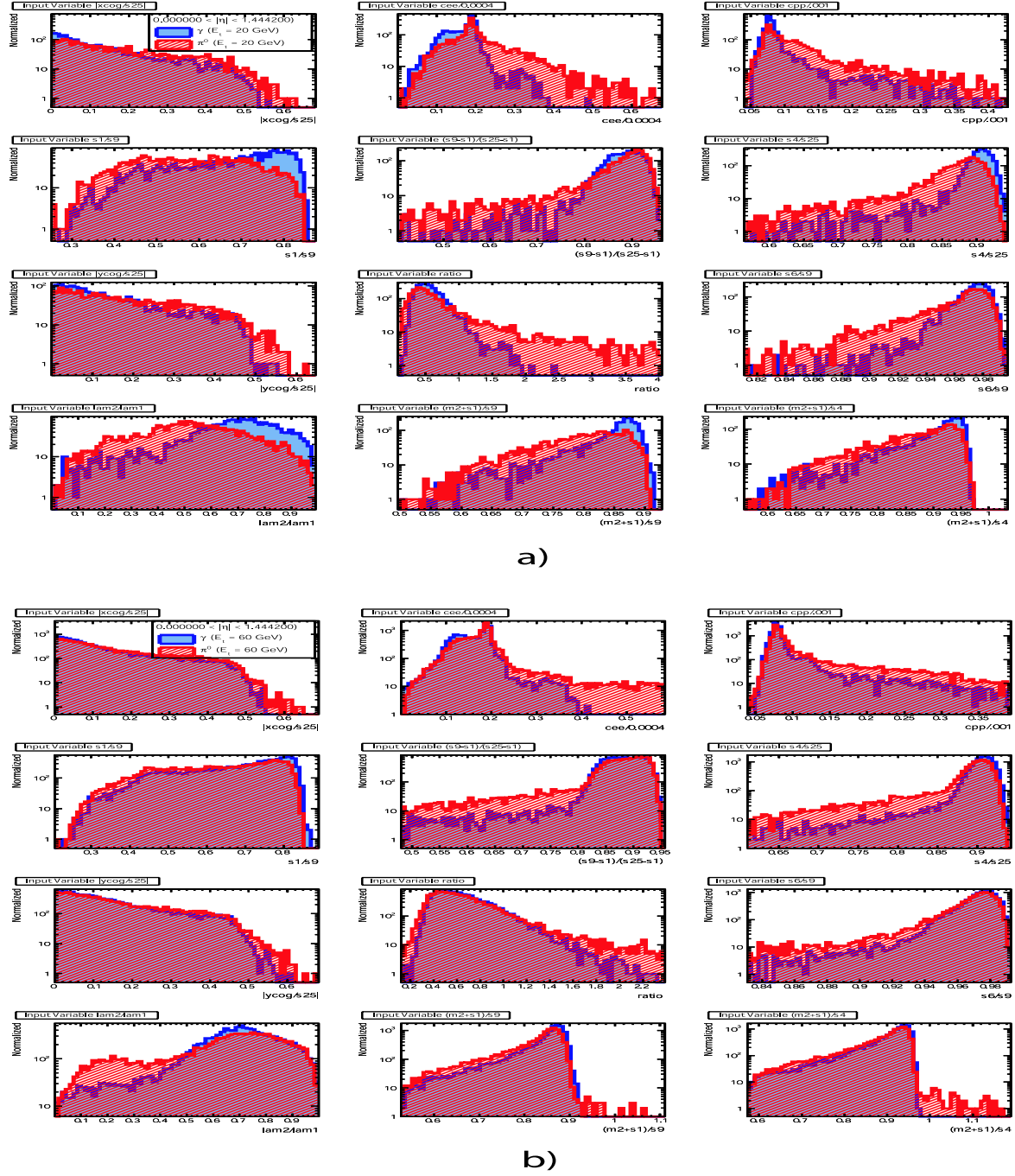


Figure 4: Input variables for ECAL Barrel photons and π^0 s with E_T 20 GeV (a) and 60 GeV (b) coming from "GammaJetIsoPi0" events. The " $N_{trk}^{ConvID} = 0$ " method used for finding unconverted particles

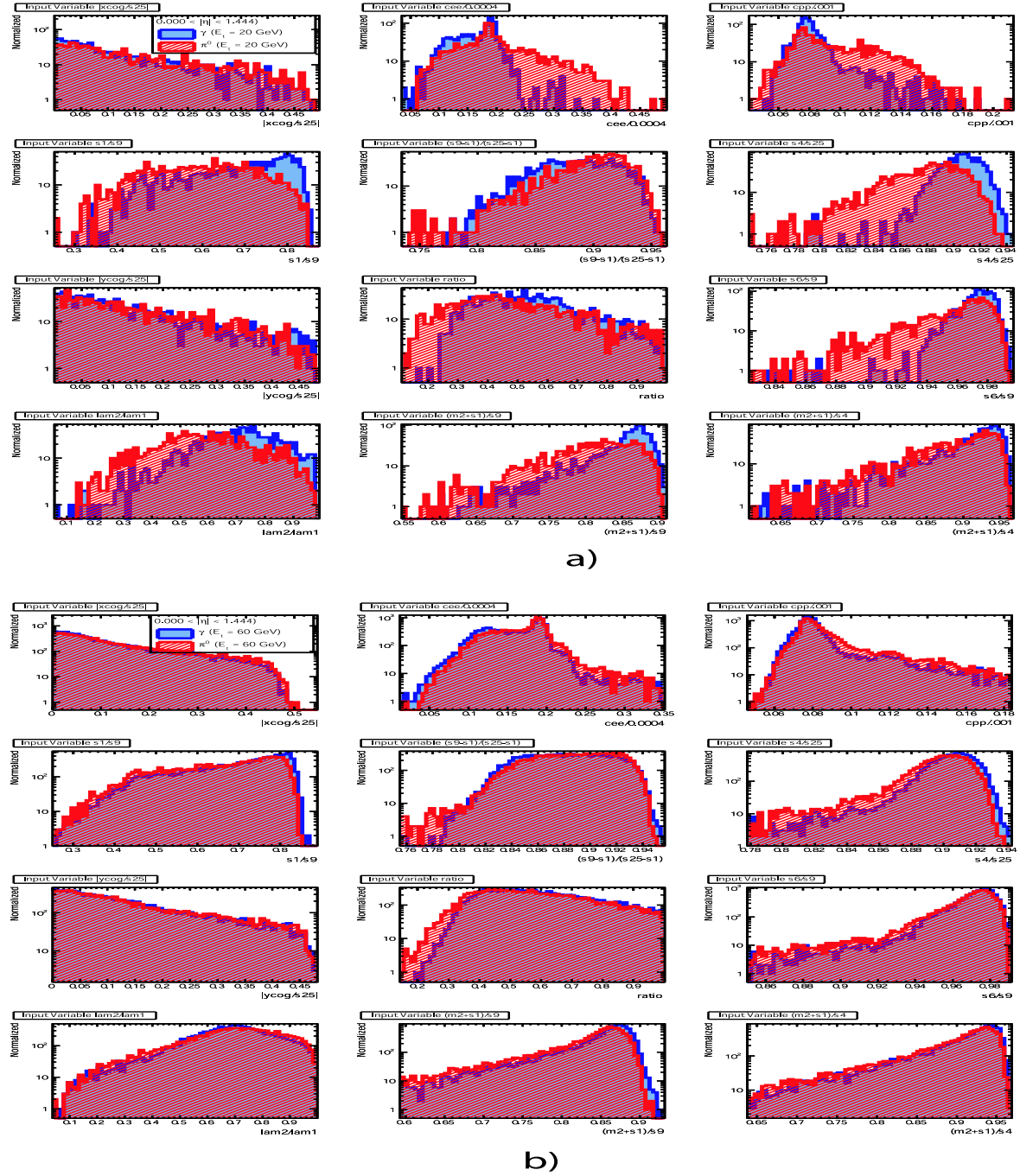


Figure 5: Input variables for ECAL Barrel photons and π^0 s with E_T 20 GeV (a) and 60 GeV (b) coming from "GammaJetIsoPi0" events. The " $R9 > 0.93$ " method used for finding unconverted particles

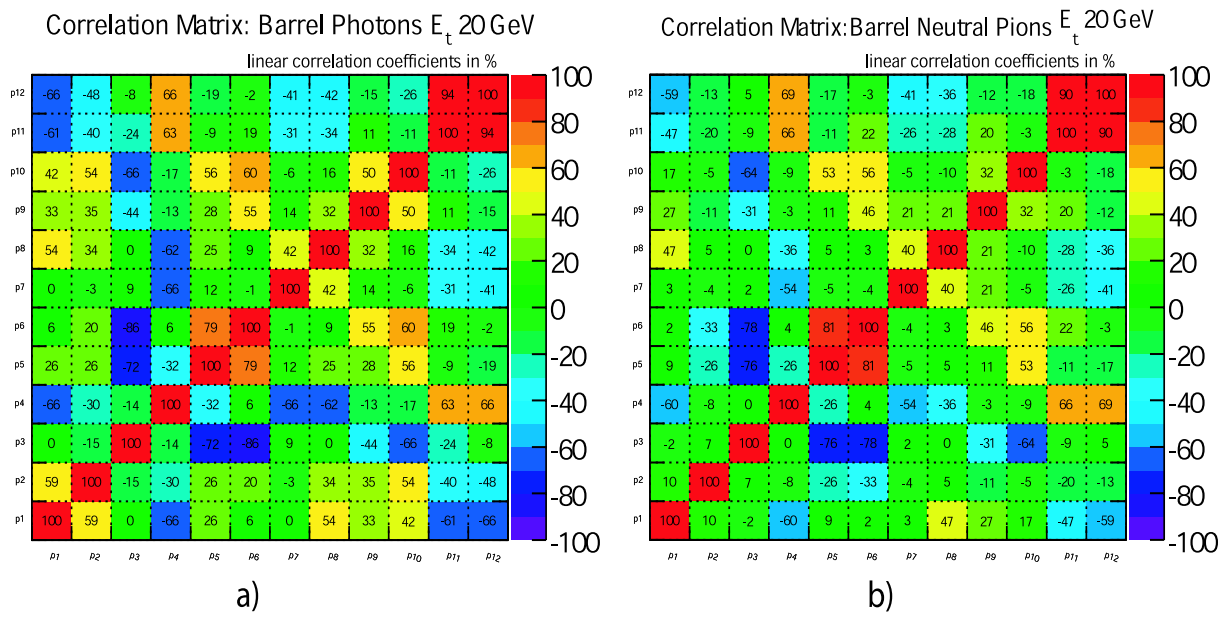


Figure 6: Correlation matrix for ECAL Barrel photons (a) and π^0 's (b) of E_T 20 GeV coming from "GammaJetI-soPi0" events. The " $N_{trk}^{ConvID} = 0$ " method used for finding unconverted particles

- we define a straight line that connects the barycenter of the ECAL endcap cluster with the point (0, 0, 0) (the origin in the CMS detector).
- we find the intersection of the above defined line with the X-Plane (X_{imp}) and Y-Plane (Y_{imp}) of the preshower.
- we store the deposited energy of the strip closest to the X_{imp} (Y_{imp}) and the energies of the ± 5 strips around this strip.

In total 11 strips were used in each plane (corresponding to 2cm arc length), which is sufficient to contain signals from π^0 's down to $E_T = 20$ GeV (Fig. 7 b).

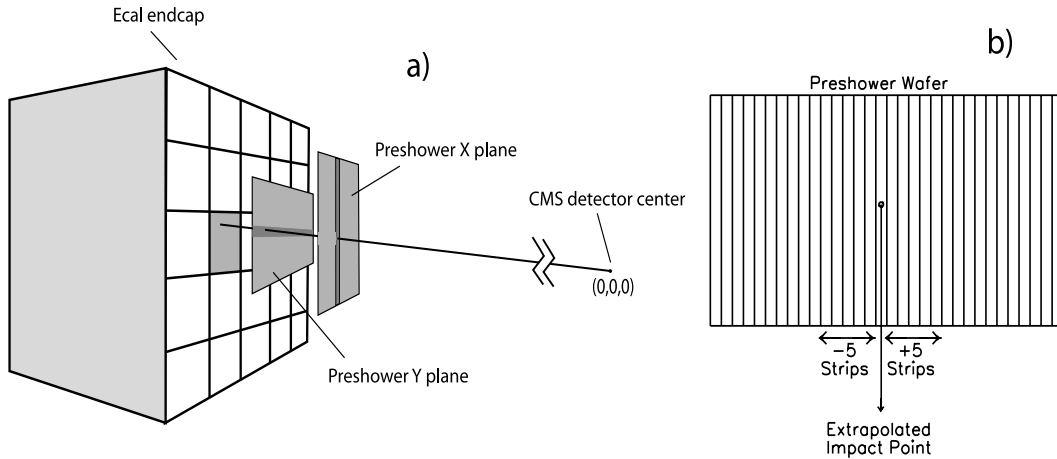


Figure 7: (a) a schematic view of how the method works for Endcap. A straight line connects the ECAL Endcap cluster barycenter with point (0,0,0) and find the intersection with two preshower planes. (b) In total 11 strips (the closest to the intersection point ± 5 strips around it) were used in the proposed method. This corresponds to about 2cm arc length, sufficient to contain signals from π^0 's down to $E_T = 20$ GeV.

The Preshower energy strip profile of isolated and unconverted (using " $N_{trk}^{ConvID} = 0$ " method) photons and π^0 's of E_T 20 GeV can be seen in figure 8 a(b) for Preshower plane X(Y) correspondingly. Obviously, there is a clear peak on photons distribution at the impact point as defined above, while the π^0 distribution is broader and has

two peaks around the impact point coming from the two photons of the π^0 decay. As we move to higher E_T this difference is less obvious as seen in figure 8 c(d) for photons and π^0 with E_T 60 GeV for Preshower plane X(Y) correspondingly. The corresponding plot for unconverted (using "R9 > 0.93" method) particles is shown in figure 9. Clearly the π^0 strip profile is much closer to the photon profile in case the unconversion method used is the "R9 > 0.93". This will influence the separation power as will be seen later.

The following 25 variables were used as inputs:

$$p_1, \dots, p_{11} = \frac{E_i^X}{C_{ES}^X} (i = 1, \dots, 11)$$

$$p_{12}, \dots, p_{22} = \frac{E_i^Y}{C_{ES}^Y} (i = 1, \dots, 11)$$

$$p_{23} = \frac{S_1^{ECAL}}{C_{ECAL}}, p_{24} = \frac{S_9^{ECAL}}{C_{ECAL}}, p_{25} = \frac{S_{25}^{ECAL}}{C_{ECAL}}$$

$$C_{ES}^X = \begin{cases} 0.02 & p_1, p_2 \text{ and } p_7 \\ 0.01 & \text{else} \end{cases}, C_{ES}^Y = \begin{cases} 0.04 & p_{12}, p_{13} \text{ and } p_{18} \\ 0.02 & \text{else} \end{cases}$$

$$C_{ECAL} = \begin{cases} 500\text{GeV} & S_{25} < 500\text{GeV} \\ 1000\text{GeV} & 500\text{GeV} < S_{25} < 1000\text{GeV} \\ 7000\text{GeV} & 1000\text{GeV} < S_{25} < 7000\text{GeV} \end{cases}$$

where, E_i^X (E_i^Y) are the energies of strip i in the X(Y) preshower planes, S_1^{ECAL} , S_9^{ECAL} , S_{25}^{ECAL} are the energies of the central crystal of the ECAL cluster, the energy sum of the 9 crystals of the ECAL cluster around S_1^{ECAL} and the energy sum of the 25 crystals of the ECAL cluster around S_{25}^{ECAL} respectively and C_{ES}^X , C_{ES}^Y and C_{ECAL} are normalization factors.

One output variable was used and was set to zero (0) for π^0 events and one (1) for photon events.

Thus the NN essentially receives a simple ordered list of strips. This means that the full pattern information is available to the network, which should then be able to build-up an average (optimum) multi-dimensional pattern for the two types of particles and thus be able to distinguish between them.

Figures 10 and 11 show a distribution of input variables (photons and π^0 s) in samples from "GammaJetIsoPi0" for particle E_T 20 and 60 GeV respectively. The first 22 variables are coming from the two Preshower planes while the last three are coming from the ECAL Endcap. Figure 12 shows the linear correlations of input variables for signal (photon) and background (π^0) events of E_T 20GeV.

5 ANN training and performance

5.1 Training datasets and performance for both ECAL Barrel and Endcap ECAL Preshower regions

For the ANN training, the "GammaJetIsoPi0" data sample was used. The number of π^0 survived the HTL2Photon and Isolation conditions in Barrel and Preshower regions for various E_T ranges is shown in Table 1 and Table 2 respectively. An equal number of photon has been also selected after HTL2Photon and Isolation conditions from the same data sample. As can be clearly seen the number of events in some cases (especially in the Preshower region) is not sufficient to be used for an efficient training of the neural network. In order to overcome the above limitation the neural network has been initialized with the weights obtained from a training with single particles events (40K per particle type per E_T bin) produced with an older version of the CMS reconstruction code where the conversion information was taken from the generation level. After the initialization the network has been retrained for each E_T range using half of photons/ π^0 s mentioned in the tables 1 and 2 for training and half for testing.

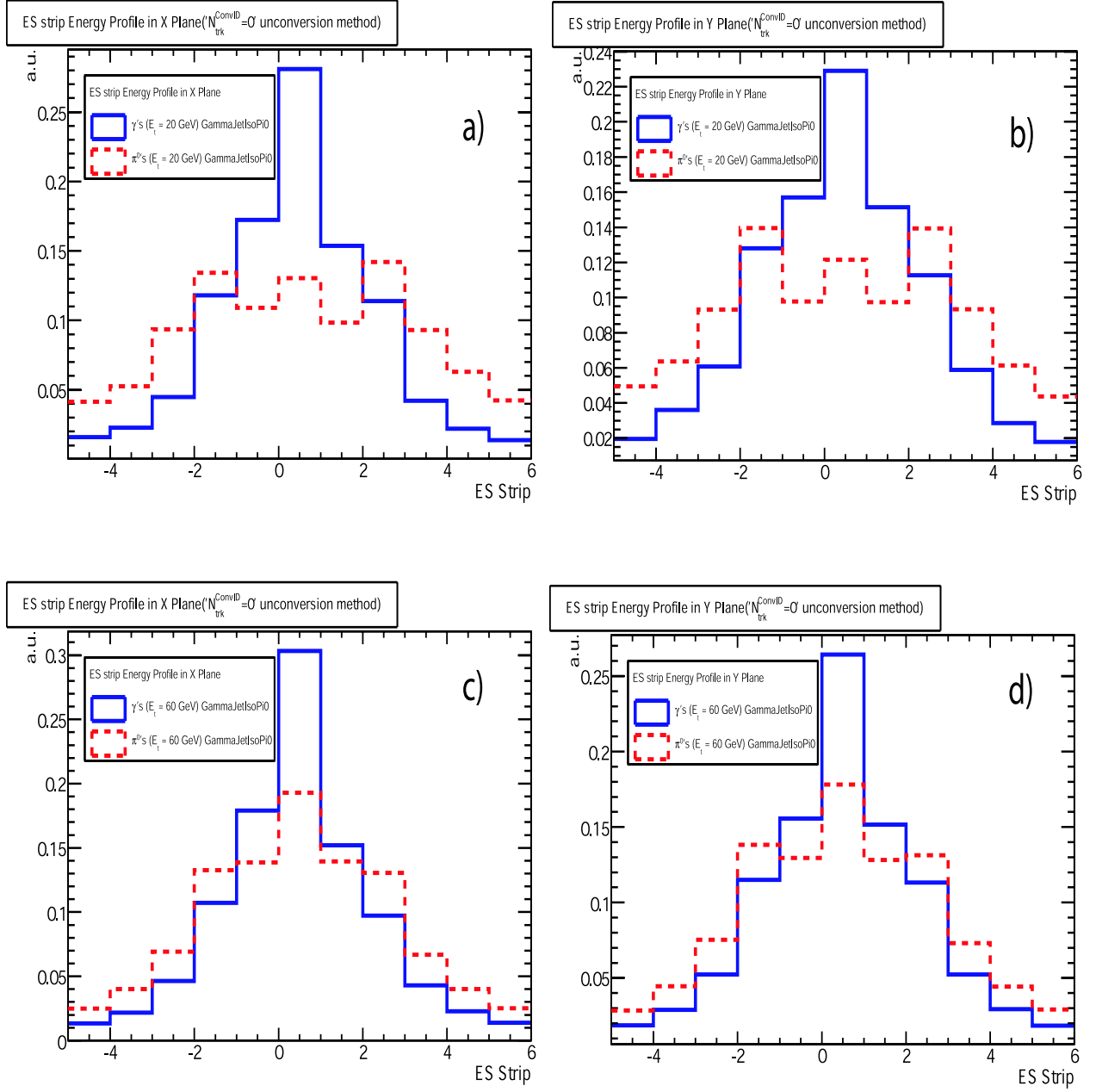


Figure 8: The Preshower (ES) energy strip profile of isolated and unconverted (using " $N_{trk}^{ConvID} = 0$ " method) photons (solid line) and π^0 's (dashed line). (a) E_T 20 GeV and X plane, (b) 20 GeV and Y plane, (c) 60 GeV and X plane and (d) 60 GeV and Y plane. Obviously, there is a clear peak on photons distribution at the intersection point as defined in the text for E_T 20 GeV in both planes (a) and (b) while the π^0 's distribution is broader and has two peaks around the intersection point coming from the two photons of the π^0 decay. As we move to higher E_T this difference is less obvious as seen in (c) and (d) for photons and π^0 's with E_T 60 GeV.

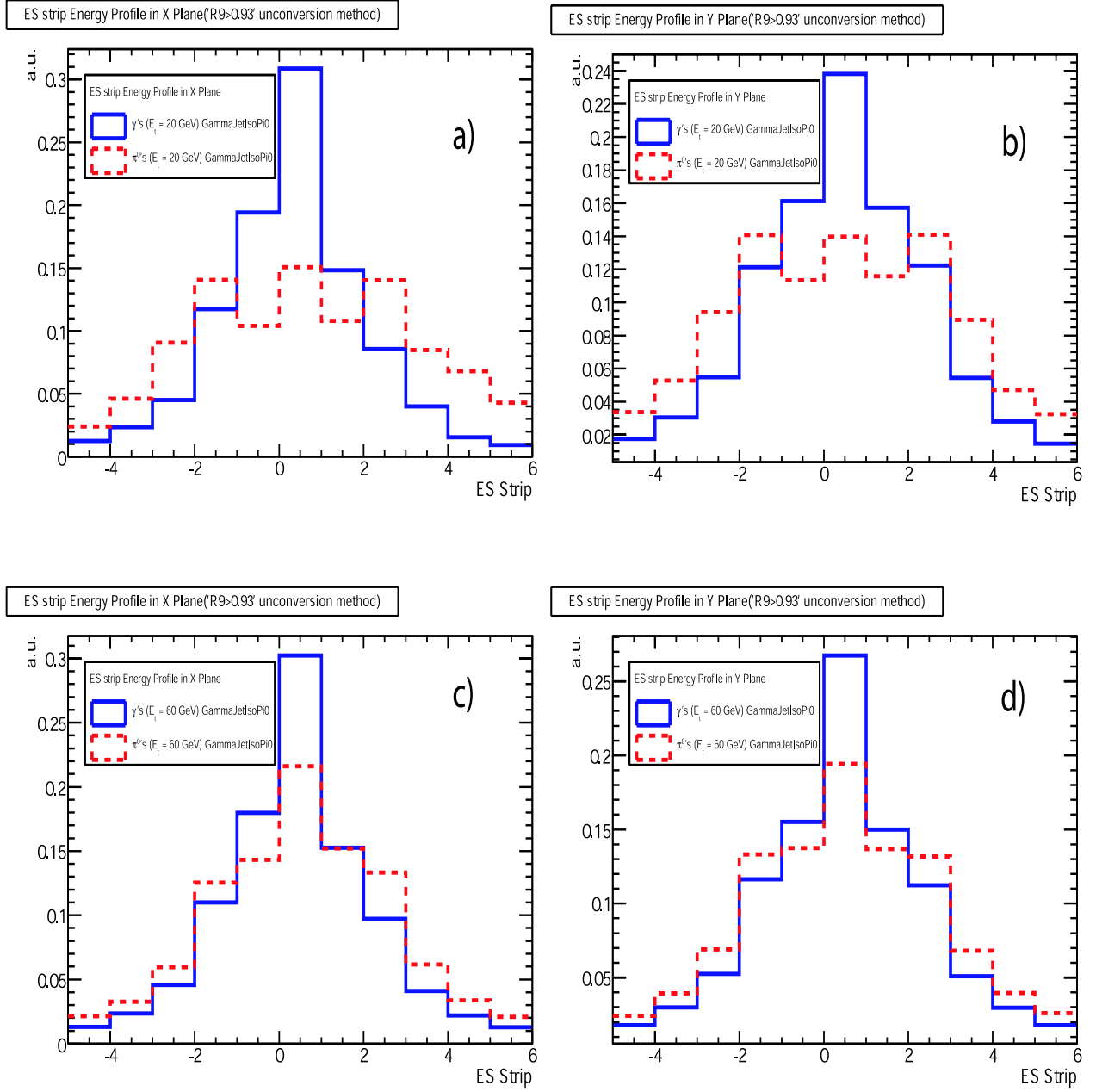


Figure 9: The Preshower (ES) energy strip profile of isolated and unconverted (using " $R9 > 0.93$ " method) photons (solid line) and π^0 's (dashed line). (a) E_T 20 GeV and X plane, (b) 20 GeV and Y plane, (c) 60 GeV and X plane and (d) 60 GeV and Y plane. Obviously, there is a clear peak on photons distribution at the intersection point as defined in the text for E_T 20 GeV in both planes (a) and (b) while the π^0 's distribution is broader and has two peaks around the intersection point coming from the two photons of the π^0 decay. As we move to higher E_T this difference is less obvious as seen in (c) and (d) for photons and π^0 's with E_T 60 GeV.

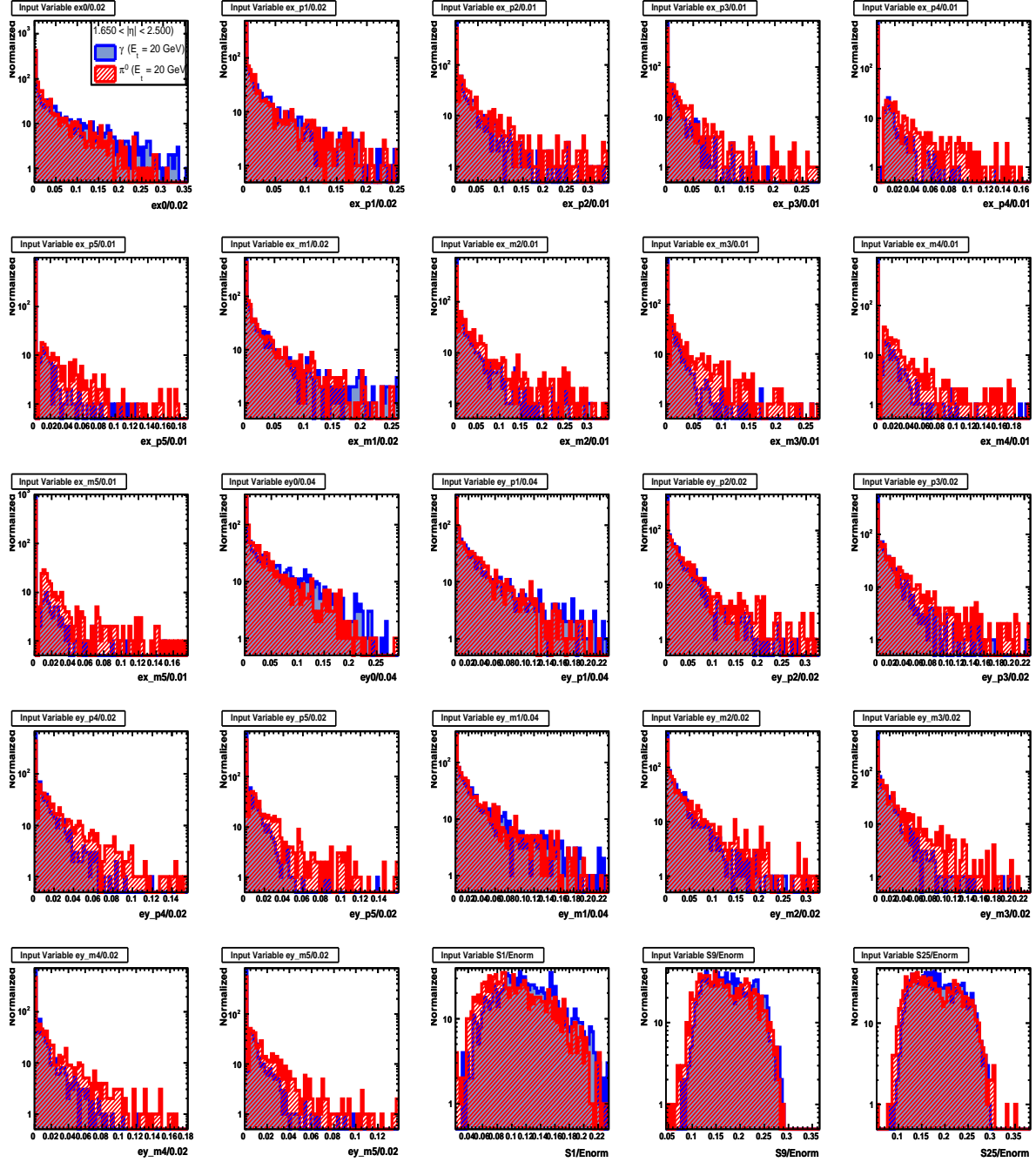


Figure 10: Input variables for E_T 20 GeV for Preshower Endcap area. The first 22 variables are coming from the two Preshower planes while the last three are coming from the ECAL Endcap. The distribution is coming from the "GammaJetIsoPi0" events. The " $N_{trk}^{ConvID} = 0$ " method used for finding unconverted particles

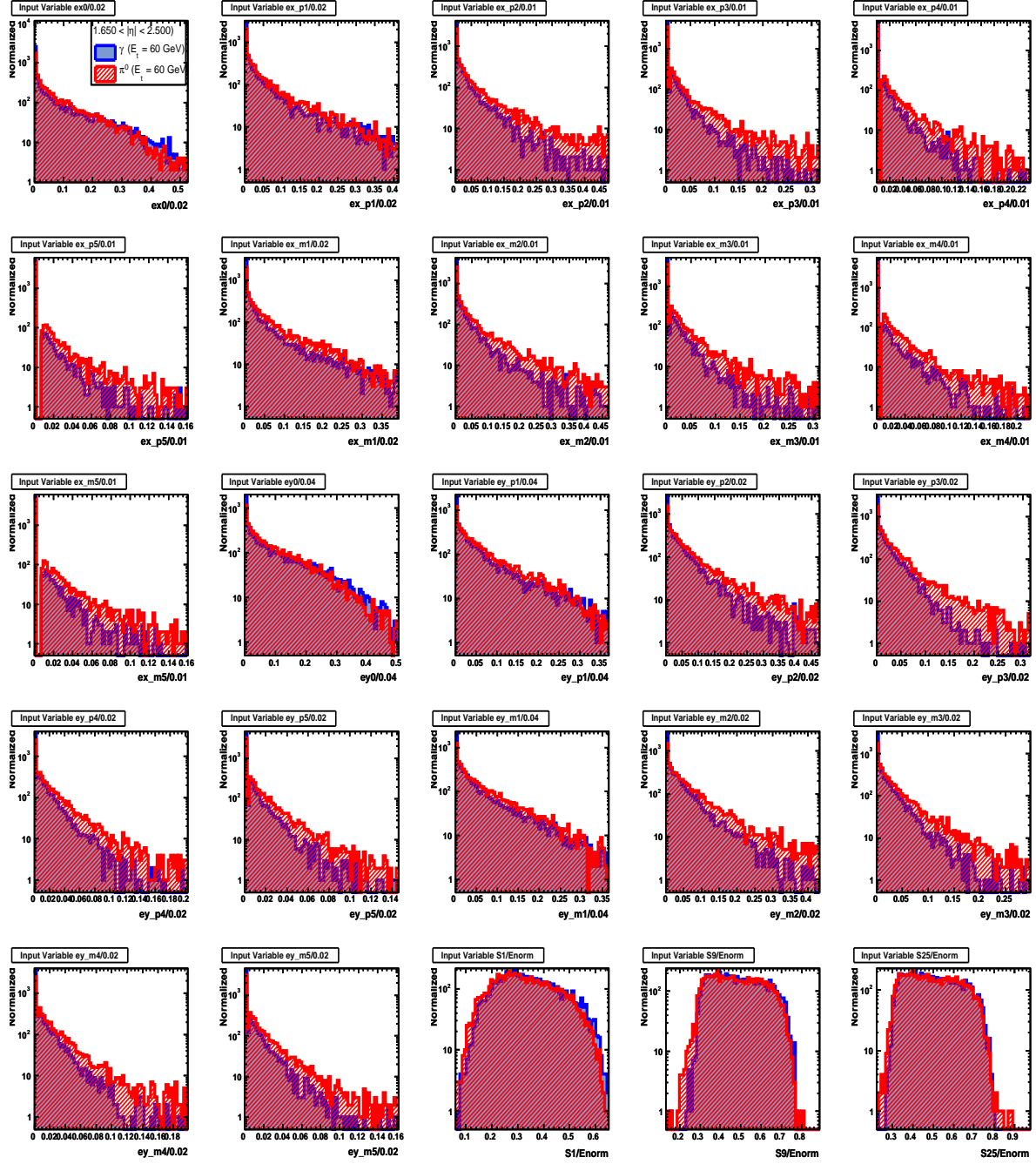
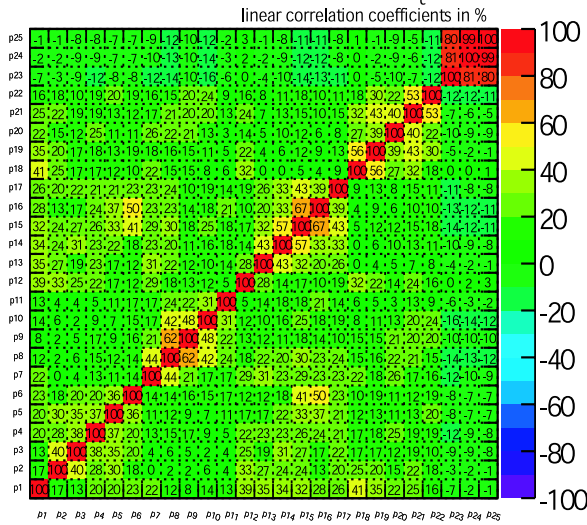


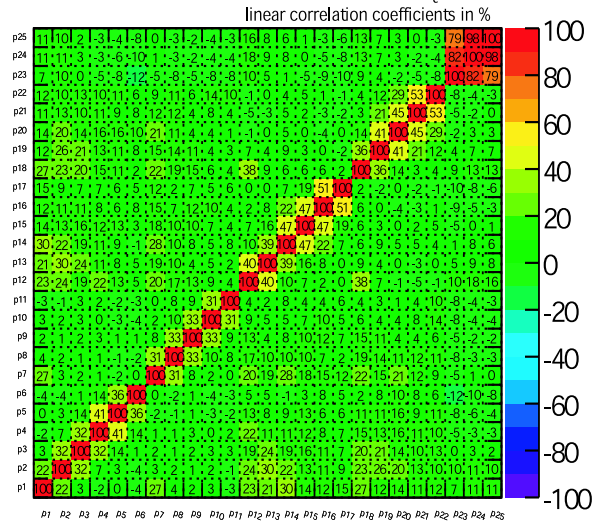
Figure 11: Input variables for E_T 60 GeV for ES Preshower Endcap area. The first 22 variables are coming from the two Preshower planes while the last three are coming from the ECAL Endcap. The distribution is coming from the "GammaJetIsoPi0" events. The " $N_{trk}^{ConvID} = 0$ " method used for finding unconverted particles

Correlation Matrix: ES Photons E_T 20 GeV



a)

Correlation Matrix: ES Neutral Pions E_T 20 GeV



b)

Figure 12: Correlation matrix for the Endcap Preshower (ES) regions photons (a) and π^0 s (b) of E_T 20 GeV. The distribution is coming from the "GammaJetIsoPi0" events. The " $N_{trk}^{ConvID} = 0$ " method is used for finding unconverted particles

TABLE 1

Number of π^0 events after HTL2Photon and Isolation cut in ECAL Barrel area per E_T bin.

E_T [GeV]	$N_{ConvID}^{trk} = 0$	$R_9 > 0.93$
20	2185	1455
30	6518	4924
40	5542	4439
50	9739	9218
60	12837	12101

TABLE 2

Number of π^0 events after HTL2Photon and Isolation cut in Preshower area per E_T bin.

E_T [GeV]	$N_{ConvID}^{trk} = 0$	$R_9 > 0.93$
20	1186	553
30	3354	1948
40	2856	1976
50	5232	4320
60	6502	5757

5.1.1 ANN performance using the " $N_{trk}^{ConvID} = 0$ " method for selecting unconverted photons

In figure 13 (a) the distribution of the NNoutput is plotted for the isolated, unconverted photons (solid line) and π^0 s (dashed line) of the Barrel ECAL region and of E_T 20 GeV. The unconverted particles are defined by using the " $N_{trk}^{ConvID} = 0$ " method described above. From the plot there is an obvious discrimination between photons and π^0 s, as can be also seen by figure 13 (b) where the photon efficiency/ π^0 rejection is plotted against NNoutput. From this last plot the π^0 rejection for 90% photon efficiency is up to 70%. The rejection is clearly degraded when we move to higher E_T as shown in figure 13 (c) where the E_T is 60 GeV. In this last case the π^0 rejection goes down to 29% for 90% photon efficiency 13 (d). This plot was produced using "GammaJetIsoPi0" events. In Table 3 we present the π^0 rejection for 90% photon efficiency in the ECAL Barrel region and for various particles' E_T ranges.

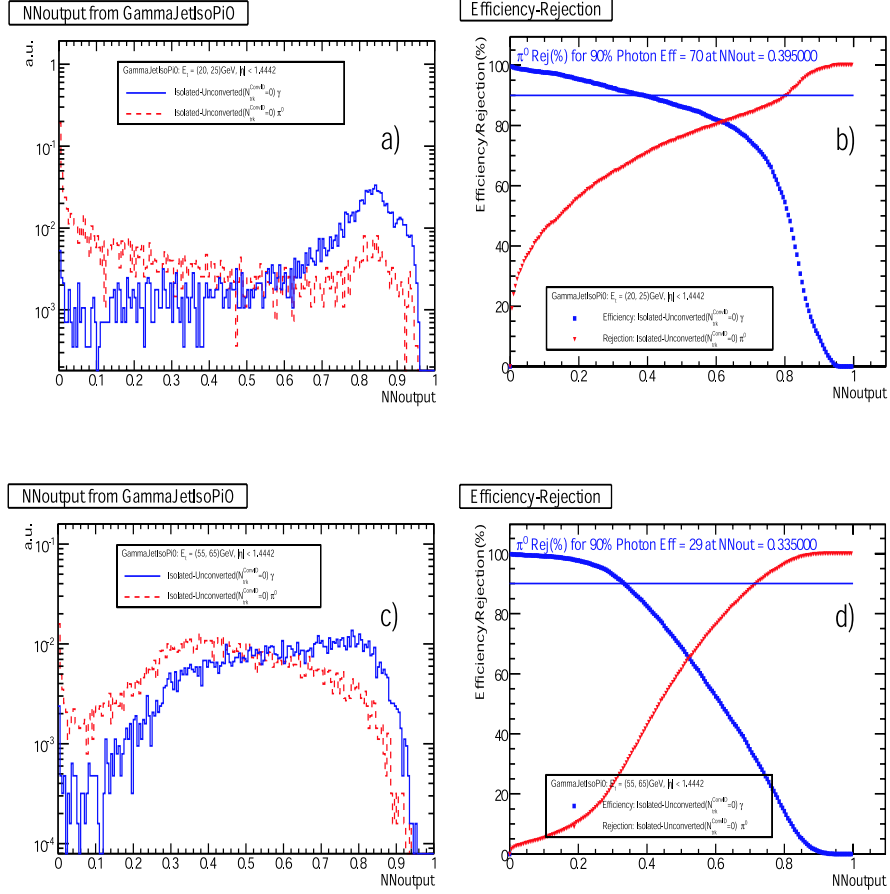


Figure 13: (a) NNoutput for isolated, unconverted ($N_{trk}^{ConvID} = 0$) photons (solid line) and π^0 s (dashed line) of the Barrel ECAL region and of E_T 20 GeV, (b) π^0 rejection (red triangle) for 90% photon efficiency (blue box) vs NNoutput for isolated, unconverted particles of E_T 20 GeV in the Barrel ECAL region. (c) NNoutput for the isolated, unconverted photons (solid line) and π^0 s (dashed line) for the Barrel ECAL region and for E_T 60 GeV, (d) π^0 rejection (red triangle) for 90% photon efficiency (blue box) vs NNoutput for isolated, unconverted particles of E_T 60 GeV in the Barrel ECAL region. The plot produced using "GammaJetIsoPi0" events.

TABLE 3

π^0 rejection for 90% photon efficiency from "GammJetIsoPi0" events for isolated and unconverted using " $N_{trk}^{ConvID} = 0$ " method particles for various E_T ranges.

	isolation and unconversion using " $N_{trk}^{ConvID} = 0$ "
E_T [GeV]	π^0 rejection for 90% photon efficiency (%)
20-25	70.0 ± 1.4
25-35	62.3 ± 0.9
35-45	43.4 ± 1.0
45-55	33.2 ± 0.7
55-65	29.3 ± 0.6

In figure 14 (a) the distribution of the NNoutput is plotted for isolated, unconverted photons (solid line) and π^0 s (dashed line) of the Endcap ECAL Preshower region and of E_T 30 GeV. The unconverted particles are defined by using the " $N_{trk}^{ConvID} = 0$ " method described above. From the plot there is an obvious discrimination between photons and π^0 s, as can be also seen by figure 14 (b) where the photon efficiency/ π^0 rejection is plotted against NNoutput. From this last plot the π^0 rejection for 90% photon efficiency is up to 62%. The rejection is clearly degraded when we move to higher E_T as shown in figure 14 (c) where the E_T is 60 GeV. In this last case the π^0 rejection goes down to 51% for 90% photon efficiency 14 (d). This plot was produced using "GammaJetIsoPi0" events. In Table 4 we present the π^0 rejection for 90% photon efficiency in the Endcap ECAL Preshower region and for various particles' E_T ranges.

TABLE 4

π^0 rejection for 90% photon efficiency from "GammJetIsoPi0" events for isolated and unconverted, using " $N_{trk}^{ConvID} = 0$ " method, particles for Endcap Preshower (ES) for various E_T ranges.

	isolation and unconversion using " $N_{trk}^{ConvID} = 0$ "
E_T [GeV]	π^0 rejection for 90% photon efficiency (%)
20-25	64.1 ± 2.0
25-35	62.1 ± 1.3
35-45	57.1 ± 1.2
45-55	54.4 ± 1.2
55-65	51.8 ± 1.0

5.1.2 ANN performance using the " $R_9 > 0.93$ " method for selecting unconverted photons

In figure 15 (a) the distribution of the NNoutput is plotted for isolated, unconverted photons (solid line) and π^0 s (dashed line) of the Barrel ECAL region and of E_T 20 GeV. The unconverted particles are defined by using the " $R_9 > 0.93$ " method described above. From the plot there is an obvious discrimination between photons and π^0 s, as can be also seen by figure 15 (b) where the photon efficiency/ π^0 rejection is plotted against NNoutput. From this last plot the π^0 rejection for 90% photon efficiency is up to 76%. The rejection is clearly degraded when we move to higher E_T as shown in figure 15 (c) where the E_T is 60 GeV. In this last case the π^0 rejection goes down to 30% for 90% photon efficiency 15 (d). This plot was produced using "GammaJetIsoPi0" events. In Table 5 we present the π^0 rejection for 90% photon efficiency in the ECAL Barrel region and for various particles' E_T ranges.

TABLE 5

π^0 rejection for 90% photon efficiency from "GammJetIsoPi0" events for isolated and unconverted, using " $R_9 > 0.93$ " method, particles for ECAL Barrel for various E_T ranges.

	isolation and unconversion using " $R_9 > 0.93$ "
E_T [GeV]	π^0 rejection for 90% photon efficiency (%)
20-25	76.4 ± 1.3
25-35	67.1 ± 0.9
35-45	45.9 ± 1.0
45-55	38.2 ± 0.7
55-65	29.5 ± 0.6

In figure 16 (a) the distribution of the NNoutput is plotted for the isolated, unconverted photons (solid line) and π^0 s (dashed line) for the Endcap ECAL Preshower region and for E_T 30 GeV. The unconverted particles are defined

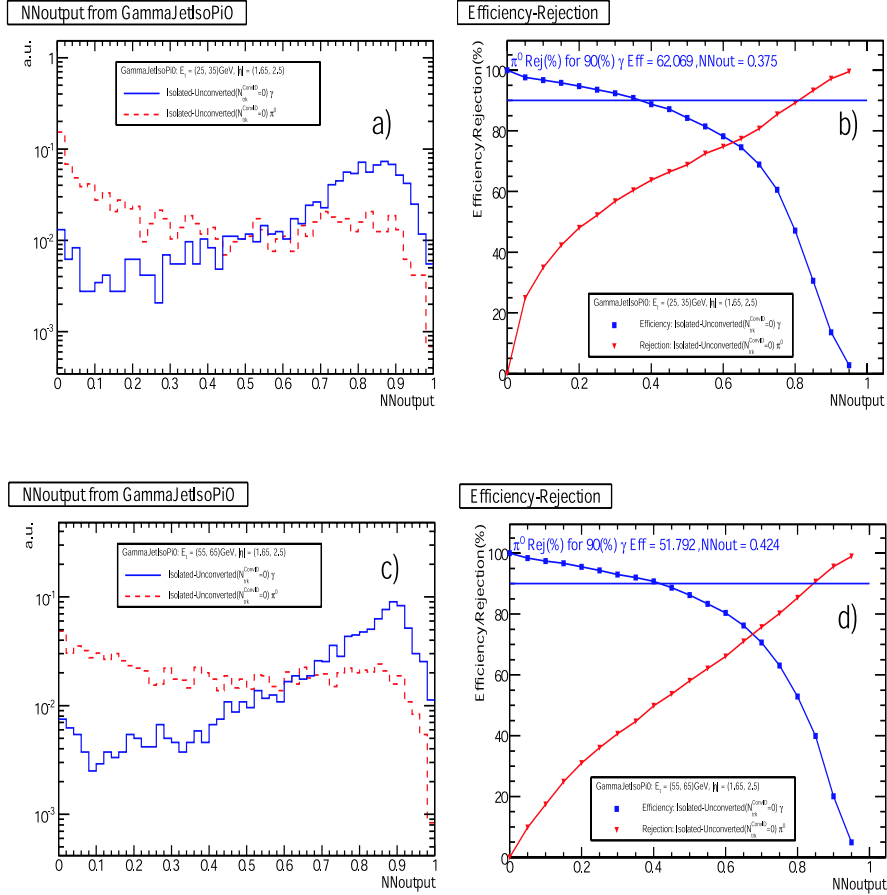


Figure 14: (a) NNOutput for isolated, unconverted ($N_{trk}^{ConvID} = 0$) photons (solid line) and π^0 s (dashed line) for the Endcap ECAL Preshower region and for E_T 30 GeV, (b) π^0 rejection (red triangle) for 90% photon efficiency (blue box) vs NNOutput for isolated, unconverted particles of E_T 30 GeV in the Endcap ECAL Preshower region. (c) NNOutput for the isolated, unconverted photons (solid line) and π^0 s (dashed line) for the Endcap ECAL Preshower region and for E_T 60 GeV, (d) π^0 rejection (red triangle) for 90% photon efficiency (blue box) vs NNOutput for isolated, unconverted particles of E_T 60 GeV in the Endcap ECAL Preshower region. The plot produced using "GammaJetIsoPi0" events.

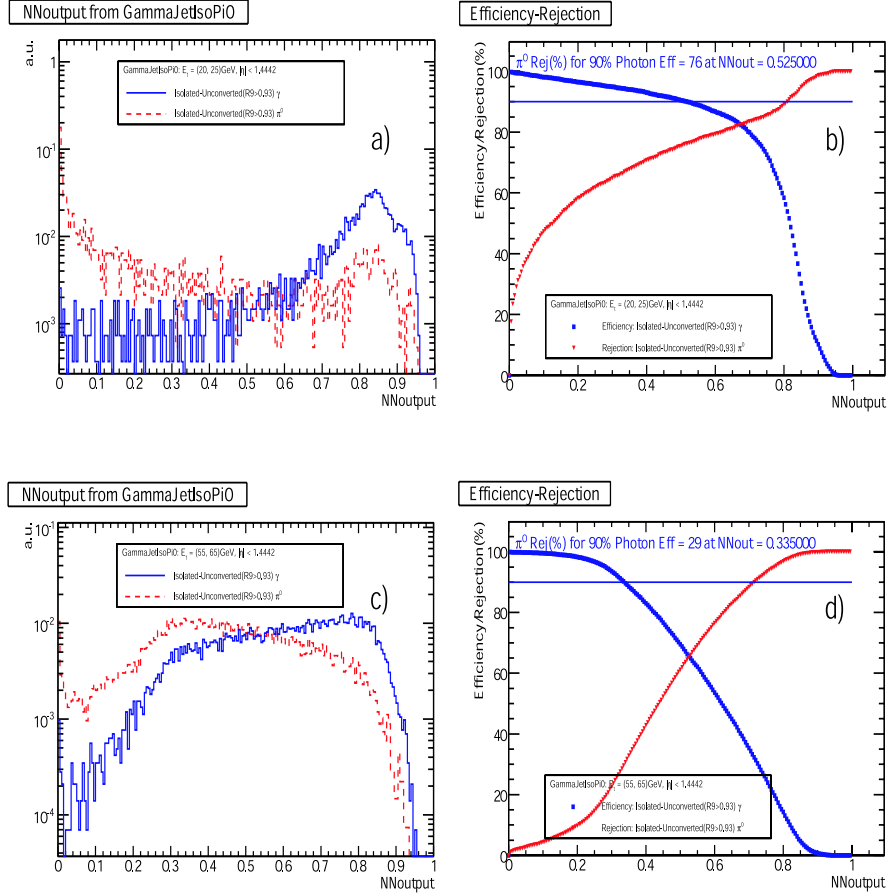


Figure 15: (a) NNOutput for isolated, unconverted (" $R9 > 0.93$ " method) photons (solid line) and π^0 s (dashed line) for the Barrel ECAL region and for E_T 20 GeV, (b) π^0 rejection (red triangle) for 90% photon efficiency (blue box) vs NNOutput for isolated, unconverted particles of E_T 20 GeV in the Barrel ECAL region. (c) NNOutput for the isolated, unconverted photons (solid line) and π^0 s (dashed line) for the Barrel ECAL region and for E_T 60 GeV, (d) π^0 rejection (red triangle) for 90% photon efficiency (blue box) vs NNOutput for isolated, unconverted particles of E_T 60 GeV in the Barrel ECAL region. The plot produced using "GammaJetIsoPi0" events.

by using the " $R9 > 0.93$ " method described above. From the plot there is an obvious discrimination between photons and π^0 s, as can be also seen by figure 16 (b) where the photon efficiency/ π^0 rejection is plotted against NNoutput. From this last plot the π^0 rejection for 90% photon efficiency is up to 55%. The rejection is clearly degraded when we move to higher E_T as shown in figure 16 (c) where the E_T is 60 GeV. In this last case the π^0 rejection goes down to 43% for 90% photon efficiency 16 (d). This plot was produced using "GammaJetIsoPi0" events. In Table 6 we present the π^0 rejection for 90% photon efficiency in the Endcap ECAL Preshower region and for various particles' E_T ranges.

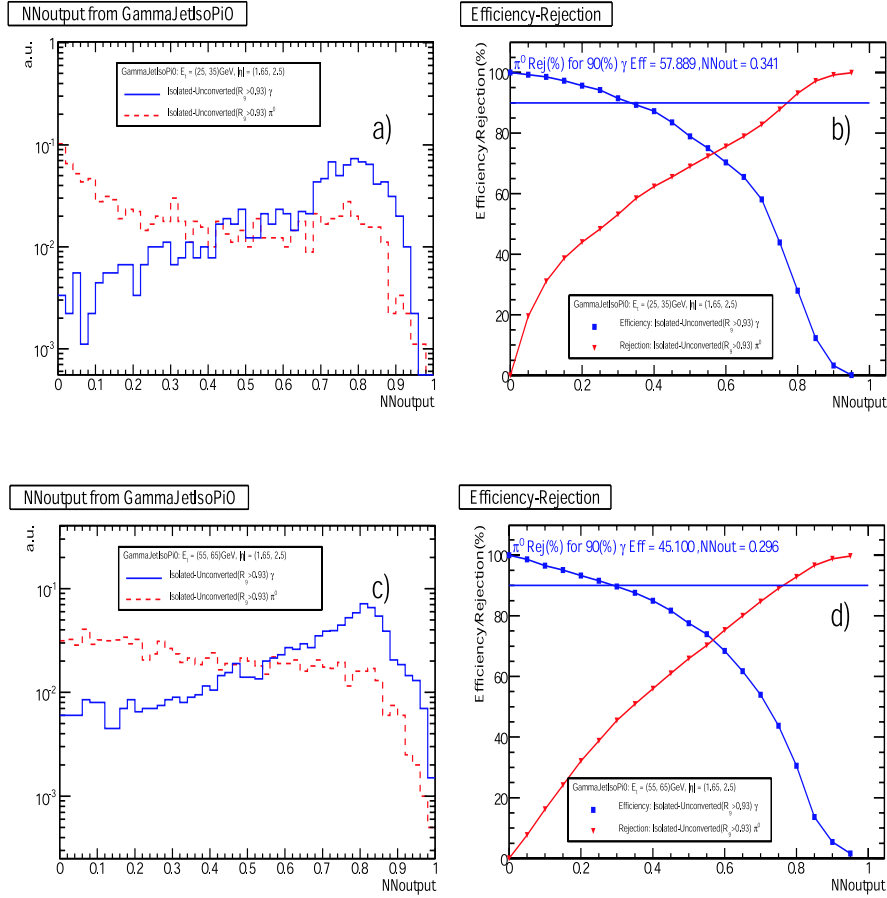


Figure 16: (a) NNoutput for the isolated, unconverted (" $R9 > 0.93$ " method) photons (solid line) and π^0 s (dashed line) for the Endcap ECAL Preshower region and for E_T 30 GeV, (b) π^0 rejection (red triangle) for 90% photon efficiency (blue box) vs NNoutput for isolated, unconverted particles of E_T 30 GeV in the Endcap ECAL Preshower region. (c) NNoutput for the isolated, unconverted photons (solid line) and π^0 s (dashed line) for the Endcap ECAL Preshower region and for E_T 60 GeV, (d) π^0 rejection (red triangle) for 90% photon efficiency (blue box) vs NNoutput for isolated, unconverted particles of E_T 60 GeV in the Endcap ECAL Preshower region. The plot produced using "GammaJetIsoPi0" events.

TABLE 6

π^0 rejection for 90% photon efficiency from "GammaJetIsoPi0" events for isolated and unconverted using " $R_9 > 0.93$ " method particles for Endcap Preshower (ES) and various E_T ranges.

isolation and unconversion using " $R_9 > 0.93$ "	
E_T [GeV]	π^0 rejection for 90% photon efficiency (%)
20-25	55.7 ± 2.1
25-35	57.3 ± 1.3
35-45	50.1 ± 1.3
45-55	49.9 ± 1.2
55-65	45.1 ± 1.0

5.1.3 Overall Performance

In figure 17 we summarize the π^0 rejection for 90% photon efficiency vs particle's super cluster E_T . Filled boxes represent the π^0 rejection in the ECAL Barrel region for isolated and unconverted particles using " $N_{trk}^{ConvID} = 0$ " method. Filled triangles represent the π^0 rejection in the Endcap Preshower (ES) region for isolated and unconverted particles using " $N_{trk}^{ConvID} = 0$ " method. Open boxes represent the π^0 rejection in the ECAL Barrel region for isolated and unconverted particles using " $R_9 > 0.93$ " method. Open diamonds represent the π^0 rejection in the Endcap Preshower (ES) region for isolated and unconverted particles using " $R_9 > 0.93$ " method.

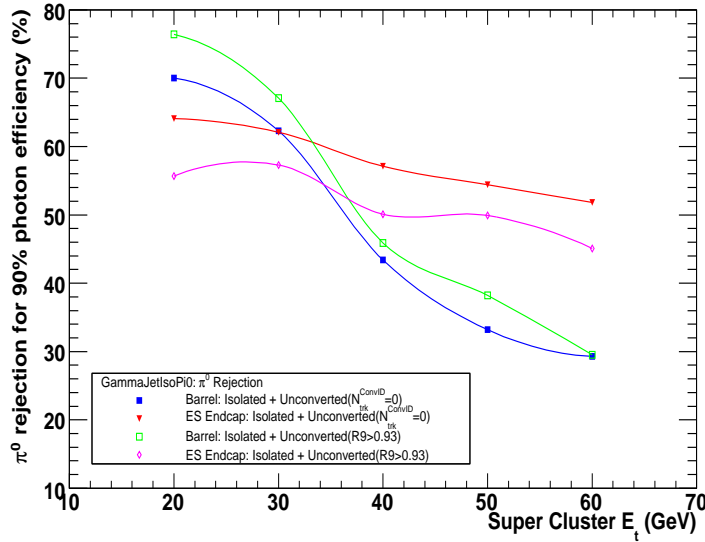


Figure 17: π^0 rejection vs super cluster E_T . Filled boxes: Barrel region for isolated and unconverted particles using " $N_{trk}^{ConvID} = 0$ " method, filled triangles: ES Endcap for isolated and unconverted particles using " $N_{trk}^{ConvID} = 0$ " method, open boxes: Barrel region for isolated and unconverted particles using " $R_9 > 0.93$ " method and open diamond: ES Endcap for isolated and unconverted particles using " $R_9 > 0.93$ " method.

A better π^0 rejection performance is observed in most of the E_T in the ECAL Barrel region for the " $R_9 > 0.93$ " method while this is reversed in the Preshower region. The first can be explained by the better separation that can be achieved by some variables like $c_{\eta\eta}/0.0004$ or s_4/s_{25} as shown in figures 4 and 5 that seems to have a better separation power after applying the " $R_9 > 0.93$ " method for selected unconverted particles. The later could be explained by the π^0 strip profile shown in figures 8 and 9 where clearly is much closer to the photon profile in case the unconversion method used is the " $R_9 > 0.93$ ".

In figure 18 we plot the NNcut vs E_T . NNcut is the value of the NNoutput for which we have 90% photon efficiency and is produced using the efficiency/rejection plots that indicatively are shown in figures 13 to 15 (b) and (d). In figure 18 (a) the NNcut = $f(E_T)$ for " $N_{trk}^{ConvID} = 0$ " unconversion method is shown for both Barrel and ECAL Endcap Preshower (ES) region. Similarly, in figure 18 (b) the NNcut = $f(E_T)$ for " $R_9 > 0.93$ " unconversion method is shown.

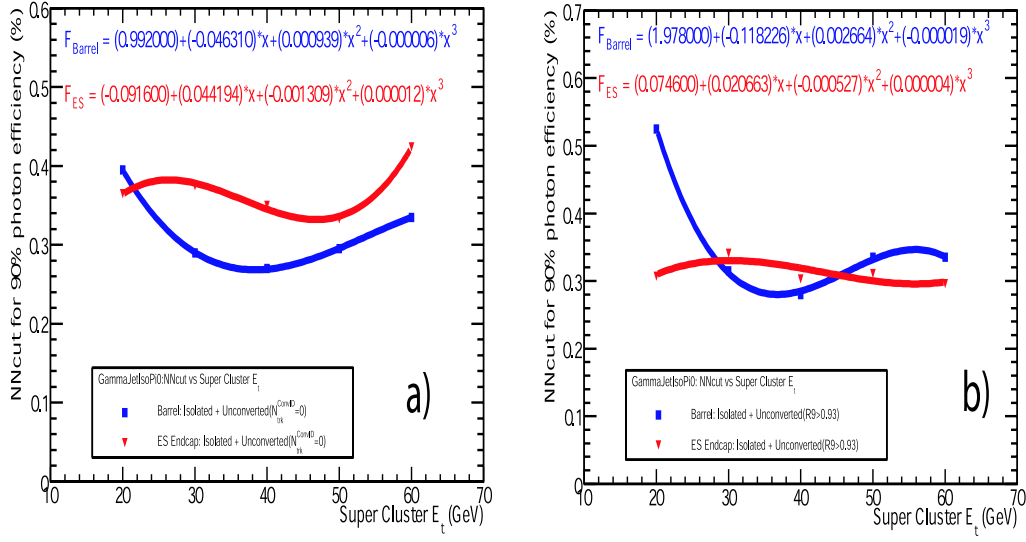


Figure 18: NNcut = $f(E_T)$ for (a) both ECAL Barrel and ECAL Endcap Preshower (ES) area using " $N_{trk}^{ConvID} = 0$ " method for defining unconverted photons and π^0 s and (b) both ECAL Barrel and ECAL Endcap Preshower (ES) area using R_9 method for defining unconverted photons and π^0 s.

5.2 Stability tests for the Neural Net

In order to test the stability of our results we performed the following tests.

5.2.1 Rejection versus training cycle

The quality of the training is controlled by means of the π^0 rejection (for 90% photon efficiency) as a function of the NN's training cycle. The results for the Barrel region are summarized in figure 19 (a) for isolated, unconverted (" $N_{trk}^{ConvID} = 0$ " method) particles and in figure 19 (b) for isolated, unconverted (" $R_9 > 0.93$ " method) particles, while the corresponding results for the Endcap ECAL Preshower region are summarized in figures 20 (a) and 20 (b). For both cases the π^0 rejection reached the optimal value after a few training cycles and remained almost stable since then.

5.2.2 Input variables strength

We checked the significance of each input variable by examining their connection strength with the nodes of the hidden layer. So, we introduced the quantity [14]:

$$SW_i = \frac{\sum_{j=1}^{N_{hidden}} |W_{ij}|}{\sum_{i=1}^{N_{input}} \sum_{j=1}^{N_{hidden}} |W_{ij}|}$$

where, W_{ij} is the weight value of the connection between the input node i and hidden node j , N_{input} is the number of input nodes and N_{hidden} is the number of hidden nodes. The larger the value of the above quantity, the stronger the contribution of the corresponding input variable to the separation. All tests were performed in samples selected as unconverted particles using the " $N_{ConvID}^{trk} = 0$ " method

5.2.3 Input variables strength ECAL Barrel region

In Tables 7,8 the relative strength of the input variables in the ECAL Barrel region is shown for particle E_t 20GeV and 60 GeV respectively and " $N_{ConvID}^{trk} = 0$ " method for selecting unconverted particles. Clearly variables like $c_{\eta\eta}/0.0004$, $c_{\phi\phi}/.001$ and s_4/s_{25} that define the "roundness" of the energy distribution in the shower play the most important role. This can be also confirmed by the input variable distributions for isolated and unconverted γ s and π^0 s shown in figure 4.

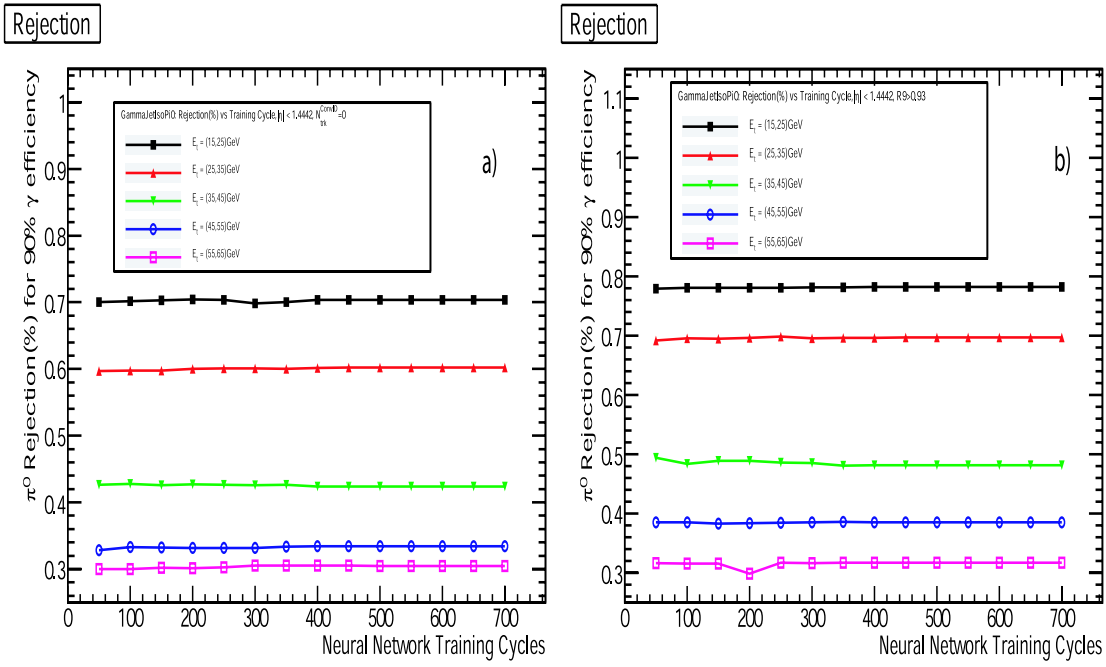


Figure 19: (a) π^0 rejection as a function of the NN's training cycle in the ECAL Barrel region, when " $N_{ConvID}^{trk} = 0$ " was used as unconversion method, (b) π^0 rejection as a function of the NN's training cycle in the ECAL Barrel region when " $R_9 > 0.93$ " was used as unconversion method

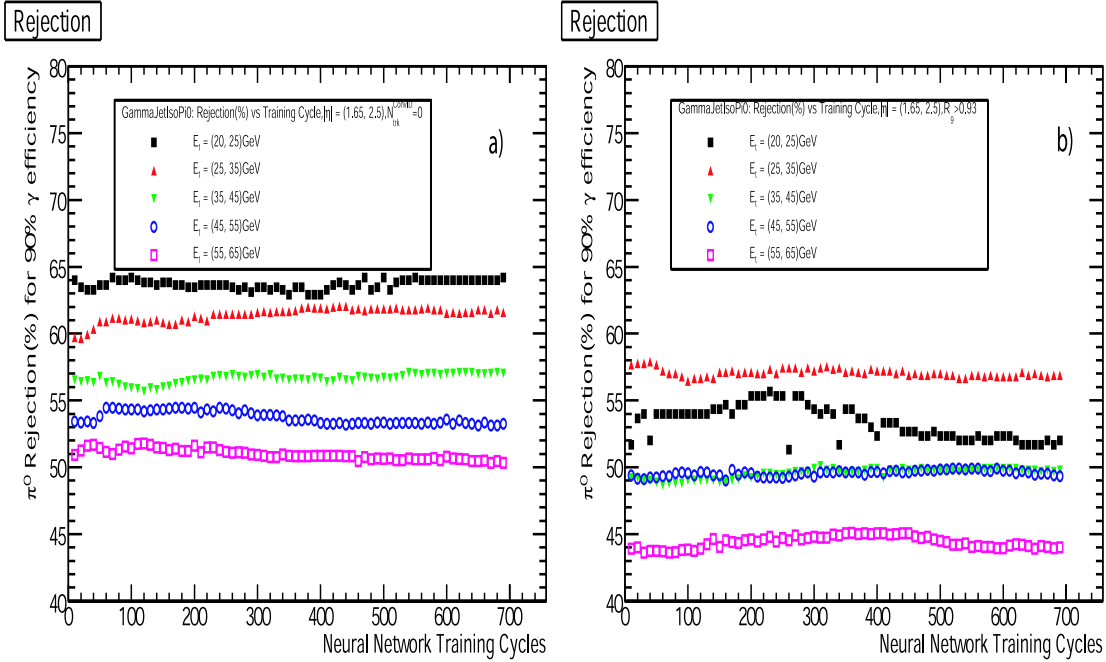


Figure 20: (a) π^0 rejection as a function of the NN's training cycle in the Endcap ECAL Preshower region when " $N_{ConvID}^{trk} = 0$ " was used as unconversion method, (b) π^0 rejection as a function of the NN's training cycle in the Endcap ECAL Preshower region when " $R_9 > 0.93$ " was used as unconversion method

TABLE 7

Strength of the input variables for ECAL Barrel region and for particle E_t 20GeV (“ $N_{ConvID}^{trk} = 0$ ” method)

Variable number	SW_i (%)	Variable name
p2	14.6015	$c_{\eta\eta}/0.0004$
p3	14.5668	$c_{\phi\phi}/.001$
p6	10.1143	s_4/s_{25}
p1	8.72915	$ x_{cog} $
p10	7.71761	λ_-/λ_+
p4	7.47729	s_1/s_9
p12	6.72707	$(m_2 + s_1)/s_4$
p5	6.69994	$(s_9 - s_1)/(s_{25} - s_1)$
p11	6.65848	$(m_2 + s_1)/s_9$
p8	6.5333	$s_{6-ratio}$
p9	5.6755	s_6/s_9
p7	4.49911	$ y_{cog} $

TABLE 8

Strength of the input variables for ECAL Barrel region and for particle E_t 60GeV (“ $N_{ConvID}^{trk} = 0$ ” method)

Variable number	SW_i (%)	Variable name
p6	20.9137	s_4/s_{25}
p3	12.8686	$c_{\phi\phi}/.001$
p1	11.9814	$ x_{cog} $
p11	9.44335	$(m_2 + s_1)/s_9$
p5	7.36019	$(s_9 - s_1)/(s_{25} - s_1)$
p4	6.81615	s_1/s_9
p10	5.66824	λ_-/λ_+
p12	5.63988	$(m_2 + s_1)/s_4$
p7	5.32904	$ y_{cog} $
p2	4.97922	$c_{\eta\eta}/0.0004$
p8	4.8358	$s_{6-ratio}$
p9	4.16453	s_6/s_9

5.2.4 Input variables strength in Preshower endcap region

In Tables 9, 10 the relative strength of the input variables in the Endcap ECAL Preshower region is shown for particle E_t 20GeV and 60 GeV respectively and “ $N_{ConvID}^{trk} = 0$ ” method for selecting unconverted particles. It is worth to mention that for lower E_t significant discrimination power is coming from Preshower strip energies at the edges of the energy profile as can be also verified by figure 8.

TABLE 9

Strength of the input variables for endcap ECAL Preshower region and for particle E_t 20GeV("N^{trk}_{ConvID} = 0" method)

Variable number	SW_i (%)	Variable name
p25	9.22261	S_{25}/E_{norm}
p24	8.06548	S_9/E_{norm}
p11	5.21572	$E_{imp-5}^X/0.01$
p22	5.1303	$E_{imp-5}^Y/0.02$
p17	4.96055	$E_{imp+5}^Y/0.02$
p1	4.01025	$E_{imp}^X/0.02$
p5	3.96891	$E_{imp+4}^X/0.01$
p6	3.90262	$E_{imp+5}^X/0.01$
p7	3.83284	$E_{imp-1}^X/0.02$
p18	3.74354	$E_{imp-1}^Y/0.04$
p12	3.72927	$E_{imp}^Y/0.04$
p2	3.67847	$E_{imp+1}^X/0.02$
p23	3.66784	S_1/E_{norm}
p20	3.46976	$E_{imp-3}^Y/0.02$
p9	3.37911	$E_{imp-3}^X/0.01$
p21	3.34167	$E_{imp-4}^Y/0.02$
p10	3.27813	$E_{imp-4}^X/0.01$
p15	3.25265	$E_{imp+3}^Y/0.02$
p4	3.24008	$E_{imp+3}^X/0.01$
p13	3.22328	$E_{imp+1}^Y/0.04$
p8	3.12368	$E_{imp-2}^X/0.01$
p19	3.06034	$E_{imp-2}^Y/0.02$
p16	2.80194	$E_{imp+4}^Y/0.02$
p3	2.52191	$E_{imp+2}^X/0.01$
p14	2.17898	$E_{imp+2}^Y/0.02$

TABLE 10

Strength of the input variables for endcap ECAL Preshower region and for particle E_t 60GeV (" $N_{ConvID}^{trk} = 0$ " method)

Variable number	SW_i (%)	Variable name
p25	7.10575	S_{25}/E_{norm}
p13	6.88639	$E_{imp+1}^Y/0.04$
p24	6.73867	S_9/E_{norm}
p18	5.86878	$E_{imp-1}^Y/0.04$
p12	5.52778	$E_{imp}^Y/0.04$
p7	5.3936	$E_{imp-1}^X/0.02$
p2	5.37858	$E_{imp+1}^X/0.02$
p1	4.7858	$E_{imp}^X/0.02$
p3	4.13801	$E_{imp+2}^X/0.01$
p14	3.89435	$E_{imp+2}^Y/0.02$
p11	3.64077	$E_{imp-5}^X/0.01$
p4	3.60966	$E_{imp+3}^X/0.01$
p20	3.45378	$E_{imp-3}^Y/0.02$
p5	3.19922	$E_{imp+4}^X/0.01$
p6	3.15042	$E_{imp+5}^X/0.01$
p19	3.15006	$E_{imp-2}^Y/0.02$
p8	3.01025	$E_{imp-2}^X/0.01$
p16	2.97936	$E_{imp+4}^Y/0.02$
p10	2.96229	$E_{imp-4}^X/0.01$
p9	2.95799	$E_{imp-3}^X/0.01$
p15	2.89504	$E_{imp+3}^Y/0.02$
p21	2.49188	$E_{imp-4}^Y/0.02$
p22	2.48941	$E_{imp-5}^Y/0.02$
p17	2.31026	$E_{imp+5}^Y/0.02$
p23	1.9819	S_1/E_{norm}

5.2.5 Training with contaminated samples

In order to check the feasibility of training the ANN with real data we studied the performance of the ANN in contaminated samples by injecting in the training sample a percentage of π^0 s into the photon sample and vice versa. In figure 21 we show indicatively how the π^0 rejection for 90% photon efficiency changes as a function of the contamination in the Preshower Endcap region. The " $N_{ConvID}^{trk} = 0$ " method is used for selecting unconverted particles. The ANN seems to behave quite stable (within statistical errors) up to 20% contamination in all E_t . For larger contamination the rejection starts gradually to degrade.

6 The Effect of the π^0 Rejection on the $H^0 \rightarrow \gamma\gamma$ and $\gamma + \text{Jet}$ background

To test π^0 rejection algorithm we used "Official Higgs" and "GammaJet" events. The latest data sample produced with a generator level filtering requiring 2 real photons or one real + one fake photon. The cross sections of these samples, the preselection cut efficiencies, the number of analyzed events as well as the expected number of events at $L = 1fb^{-1}$ are summarized in Table 11.

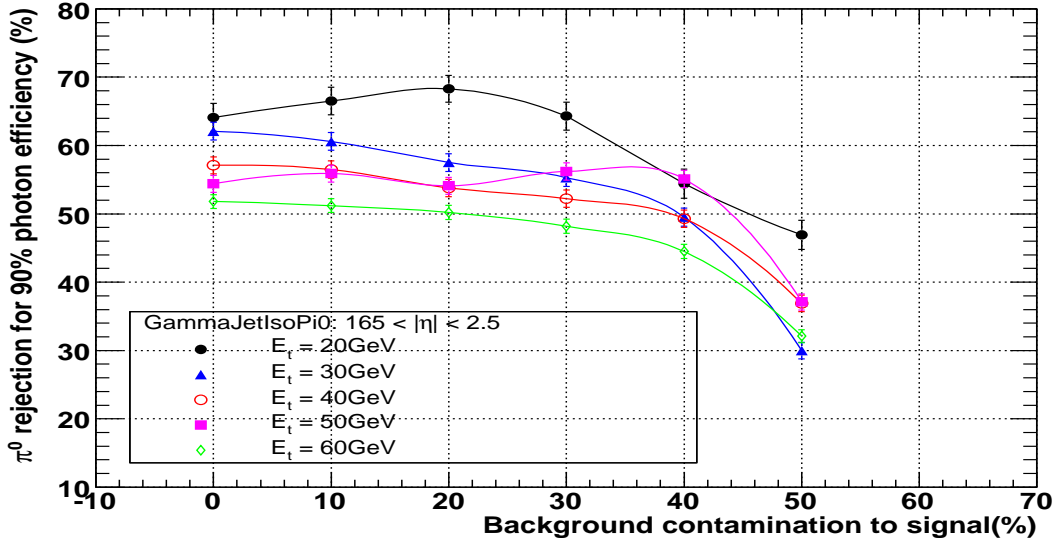


Figure 21: π^0 rejection for 90% photon efficiency as a function of the contamination of the training sample for " $N_{ConvID}^{trk} = 0$ " method for selecting unconverted particles and various E_t in the Preshower Endcap region. The errors are statistical only

TABLE 11

The cross sections, the preselection cut efficiencies, the number of analyzed events as well as the expected number of events at $L = 1fb^{-1}$ for the $\gamma + \text{Jet}$ and $H^0 \rightarrow \gamma\gamma$ samples

Data Sample	$\gamma + \text{Jet}$	$H^0 \rightarrow \gamma\gamma, M_{\gamma\gamma} = 120\text{GeV}/c^2$
Analyzed Events	1218K	253
$\sigma \times BR(pb)$	90000	0.08
Preselection Efficiency	0.0067	1
Events@ $1fb^{-1}$	603K	80
Event Weight	0.49507	0.000316
HLT2Photon	375K	79

The analysis started by applying "HLT2Photon" trigger. Its results also shown in Table 11. Then, we demanded the sample to have at least two photon candidates in the fiducial ECAL volume ($|\eta| < 2.5$ and not in the crack ECAL Barrel/Endcap region. We demand one of the photons to have $E_T > 40\text{GeV}$ and the other $E_T > 25\text{GeV}$. In figure 22 (a) the E_t spectrum of the two photons coming from the Higgs decay is plotted. The solid blue line refers to photon with the minimum E_t while the dashed red line to the photon with the maximum E_t . Similar figure 22 (b) shows the E_t spectrum of the photons (solid blue line) and π^0 s (dashed red line) coming from "GammaJet" events. The similarity of the distributions is obvious. Then, for each photon candidate we applied the tracker isolation criteria described above.

In a figure 23 (a) we plot the invariant mass of the two photons candidates for "Official Higgs" events: solid black line after the application of the E_t cuts, dashed green line after the application of the isolation cuts, dotted red line with the extra demand both of photons to be unconverted using the " $N_{trk}^{ConvID} = 0$ " method and dashed - dot blue line represents the two photon invariant mass distribution after the NNcut = $f(E_T)$ application (from figure 18). In 23 (b) we plot the ratio of the dot/dashed-dot distribution of figure shown in 23 (a). If we restrict ourselves to the region $115\text{GeV}/c^2 < M_{\gamma\gamma} < 125\text{GeV}/c^2$ we can calculate that 88% of the "Official Higgs" signal survive. The same way, in a figure 23 (c) we plot the invariant mass of the two photons candidates for "Official GammaJet". The line color and style notation is the same as in figure 23 (a). In 23 (d) we plot the ratio of the dot/dashed-dot distribution of figure shown in 23 (c). If we restrict ourselves to the region $115\text{GeV}/c^2 < M_{\gamma\gamma} < 125\text{GeV}/c^2$ we observe that 43% of the "Official GammaJet" signal survive.

So we can say that for 12% signal rejection we have 57% background rejection.

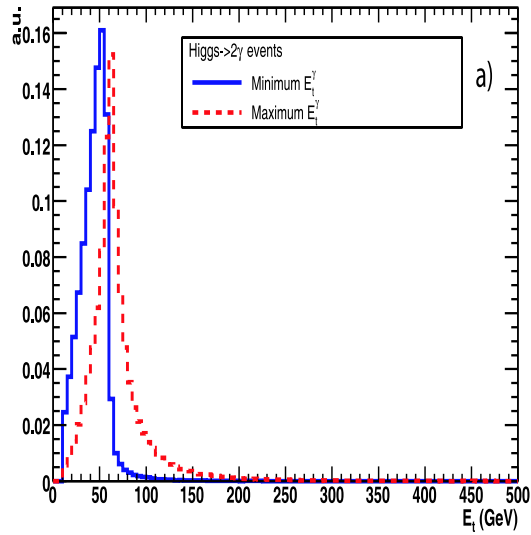
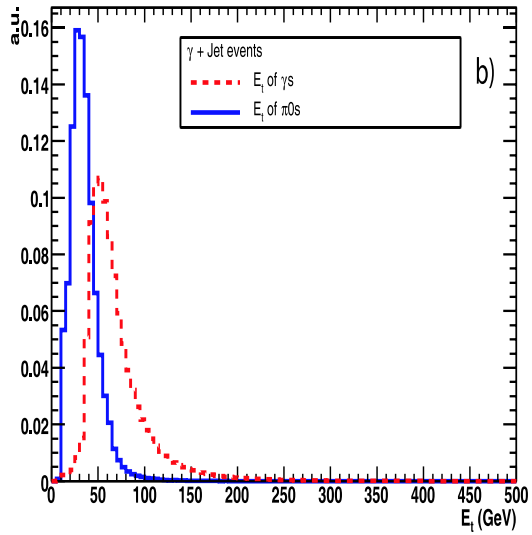
E_t of photons from Higgs \rightarrow 2 γ  **E_t of photons and π^0 s from γ + Jet**

Figure 22: (a) E_t of photon candidates coming from the "Official Higgs" events. Solid blue line: matched to photon from Higgs decay with the minimum E_t . Dashed red line: matched to photon from Higgs decay with the maximum E_t . (b) E_t of photon candidates coming from the "GammaJet" events. Solid blue line: matched to the photon. Dashed red line: matched to the π^0

In a figure 24 (a) we plot the invariant mass of the two photons candidates for "Official Higgs" events: solid black line after the application of the E_t cuts, dashed green line after the application of the isolation cuts, dotted red line with the extra demand both of photons to be unconverted using the " $R_9 > 0.93$ " method and dashed - dot blue line represents the two photon invariant mass distribution after the NNcut = $f(E_T)$ application (from figure 18). In 24 (b) we plot the ratio of the dot/dashed-dot distribution of figure shown in 24 (a). If we restrict ourselves to the region $115\text{GeV}/c^2 < M_{\gamma\gamma} < 125\text{GeV}/c^2$ we can calculate that 85% of the "Official Higgs" signal survive. The same way, in a figure 24 (c) we plot the invariant mass of the two photons candidates for "Official GammaJet". The line color and style notation is the same as in figure 24 (a). In 24 (d) we plot ratio of the dot/dashed-dot distribution of figure shown in 24 (c). If we restrict ourselves to the region $115\text{GeV}/c^2 < M_{\gamma\gamma} < 125\text{GeV}/c^2$ we observe that 54% of the "Official GammaJet" signal survive. The distributions 24 (a), (c) are normalized to $L = 1\text{fb}^{-1}$

So we can say that for 15% signal rejection we have 46% background rejection.

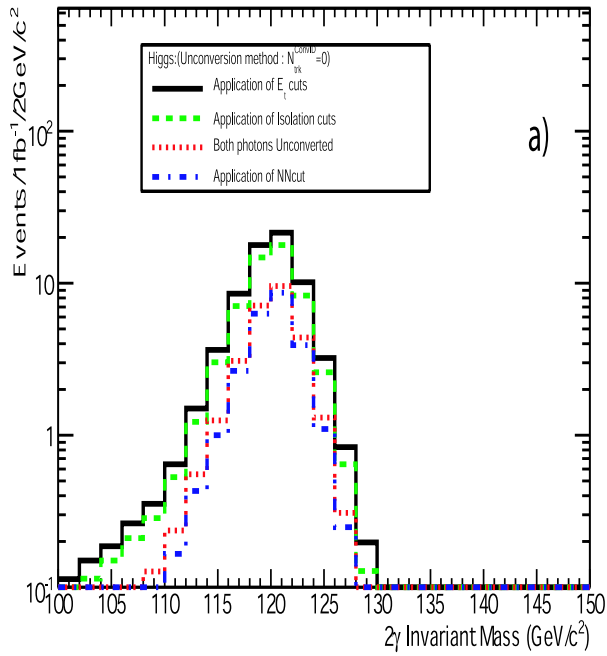
In Table 12 we summarize the cut efficiency restricting ourselves to the two photon mass region of $115\text{GeV}/c^2 < M_{\gamma\gamma} < 125\text{GeV}/c^2$ and for $L = 1\text{fb}^{-1}$. Notice that the numbers and percentages in line (3a) and (4a) are taken with respect to line (2) while those of lines (3b) and (4b) with respect to (3a) and (4a) respectively. From this table it is obvious the the combination of " $R_9 > 0.93$ " method for selecteing unconverted photon candidate following by the application of the corresponding NNcut = $f(E_T)$ has the best results in reducing the "GammaJet" background while keeping the same number of "Higgs" events.

TABLE 12

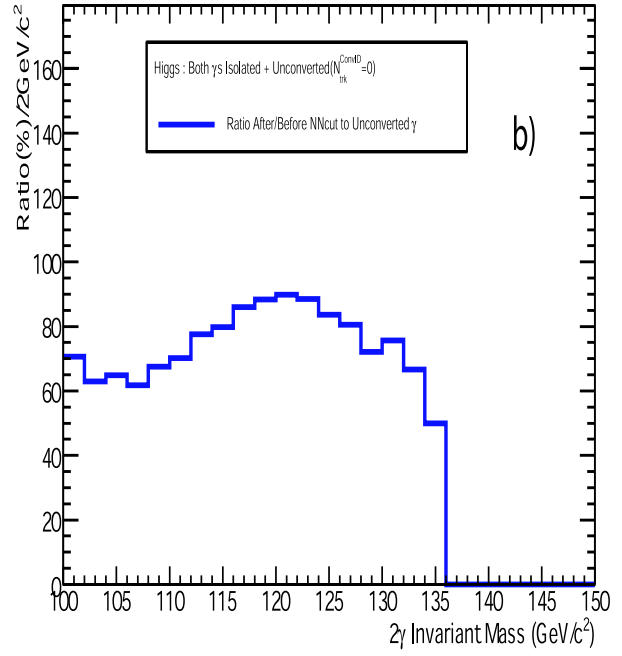
Cut efficiencies and the the number of survived events at $L = 1\text{fb}^{-1}$ for the γ + Jet and $H^0 \rightarrow \gamma\gamma$ samples

Events@ 1fb^{-1} with $115\text{GeV}/c^2 < M_{\gamma\gamma} < 125\text{GeV}/c^2$	γ + Jet	$H^0 \rightarrow \gamma\gamma, M_{\gamma\gamma} = 120\text{GeV}/c^2$
(1) $E_T^{\gamma 1} > 40\text{GeV}, E_T^{\gamma 2} > 25\text{GeV}, \eta$ in fiducial	10680	62
(2) Both Photons Isolated	1513(14%)	51(84%)
(3a) Both Unconverted ($N_{trk}^{ConvID} = 0$)	543(36%)	26(51%)
(4a) NNcut = $f(E_T)$ for (3a)	236(43%)	23(88%)
(3b) Both Unconverted ($R_9 > 0.93$)	292(20%)	27(53%)
(4b) NNcut = $f(E_T)$ for (3b)	158(54%)	23(85%)

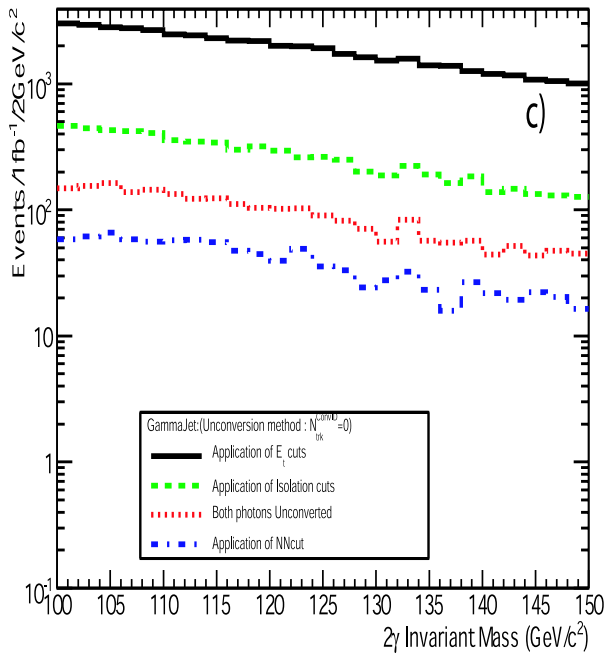
2 γ Invariant Mass from Higgs



Ratio of 2 γ Invariant Mass from Higgs after/before NNcut



2 γ Invariant Mass from GammaJet



Ratio of 2 γ Invariant Mass from GammaJet after/before NNcut

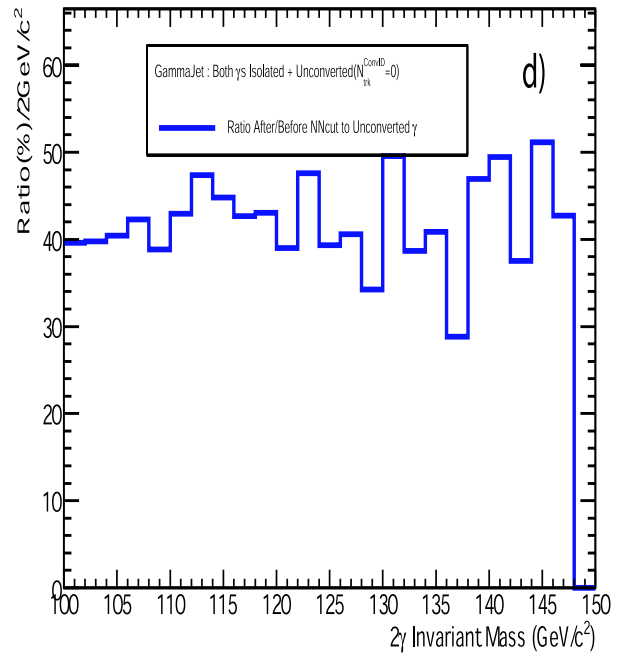
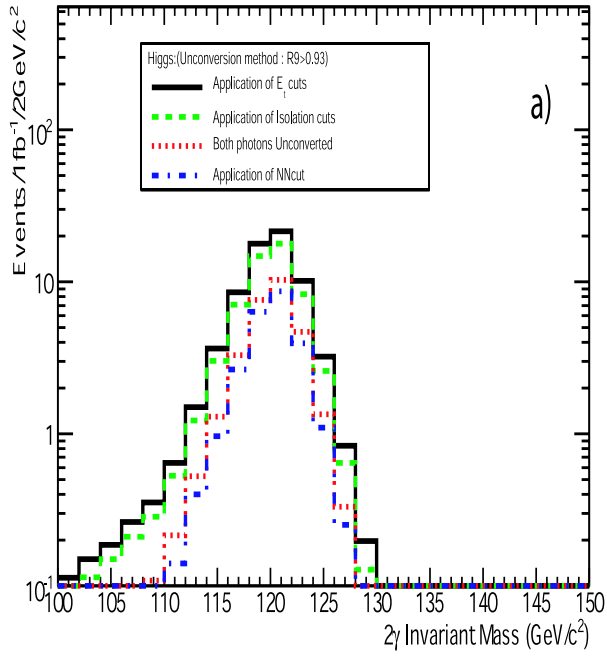
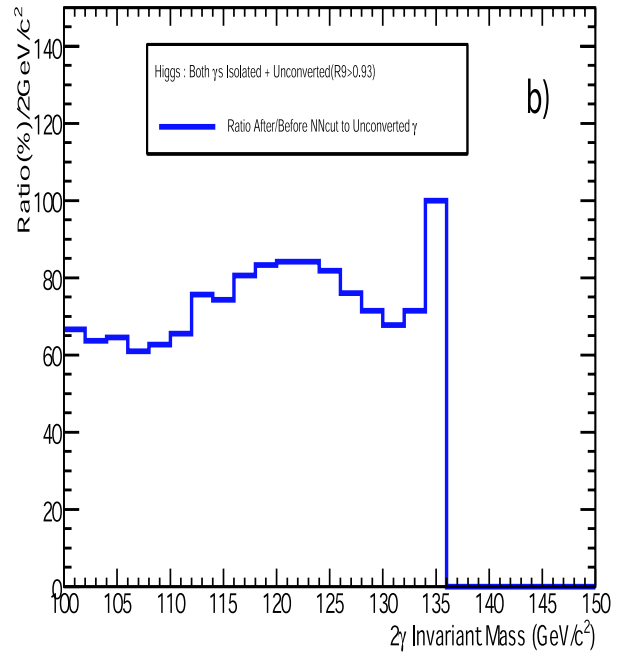


Figure 23: (a) Two photon invariant mass distribution for "Official Higgs" events after E_t cuts (solid black line), after isolation cuts (dashed green line), after the extra demand both of them to be unconverted using the " $N_{trk}^{ConvID} = 0$ " method (dotted red line) and after the NNcut = $f(E_T)$ application (dashed - dot blue line), (b) Ratio of dot/dashed-dot distributions of (a), (c) Two photon invariant mass distribution for "Official GammaJet" events after E_t cuts (solid black line), after isolation cuts (dashed green line), after the extra demand both of them to be unconverted using the " $N_{trk}^{ConvID} = 0$ " method (dotted red line) and after the NNcut = $f(E_T)$ application (dashed - dot blue line), (d) Ratio of dot/dashed-dot distributions of (d). The distributions (a), (c) are normalized to $L = 1fb^{-1}$

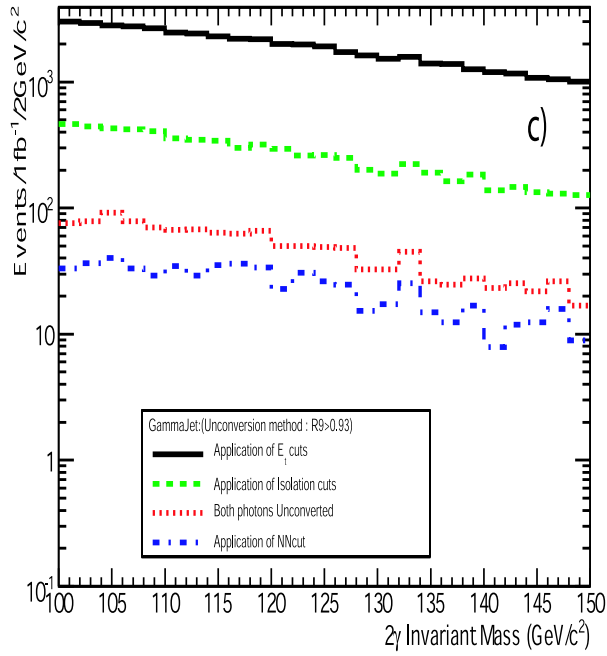
2 γ Invariant Mass from Higgs



Ratio of 2 γ Invariant Mass from Higgs after/before NNcut



2 γ Invariant Mass from GammaJet



Ratio of 2 γ Invariant Mass from GammaJet after/before NNcut

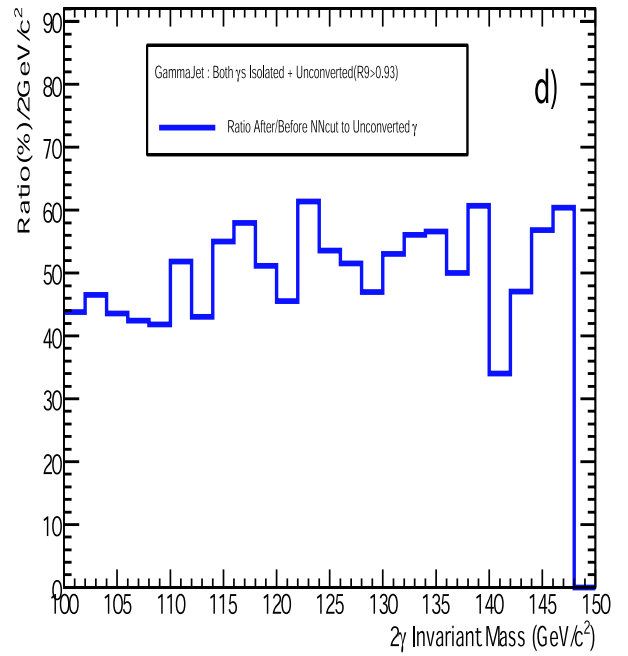


Figure 24: (a) Two photon invariant mass distribution for "Official Higgs" events after E_t cuts (solid black line), after isolation cuts (dashed green line), after the extra demand both of them to be unconverted using the " $R_9 > 0.93$ " method (dotted red line) and after the NNcut = $f(E_T)$ application (dashed - dot blue line), (b) Ratio of dot/dashed-dot distributions of (a), (c) Two photon invariant mass distribution for "Official GammaJet" events after E_t cuts (solid black line), after isolation cuts (dashed green line), after the extra demand both of them to be unconverted using the " $N_{trk}^{ConvID} = 0$ " method (dotted red line) and after the NNcut = $f(E_T)$ application (dashed - dot blue line), (d) Ratio of dot/dashed-dot distributions of (d). The distributions (a), (c) are normalized to $L = 1 fb^{-1}$

7 Trying to train the ANN from data

It is very challenging to find a way to train the ANN from real data samples, when they become available. This implies finding a source as pure as possible of photons and π^0 s. Taking into account the stability of the ANN in contaminating samples as demonstrated in section 5.2.5, we propose the following method for trying to train the ANN from real data:

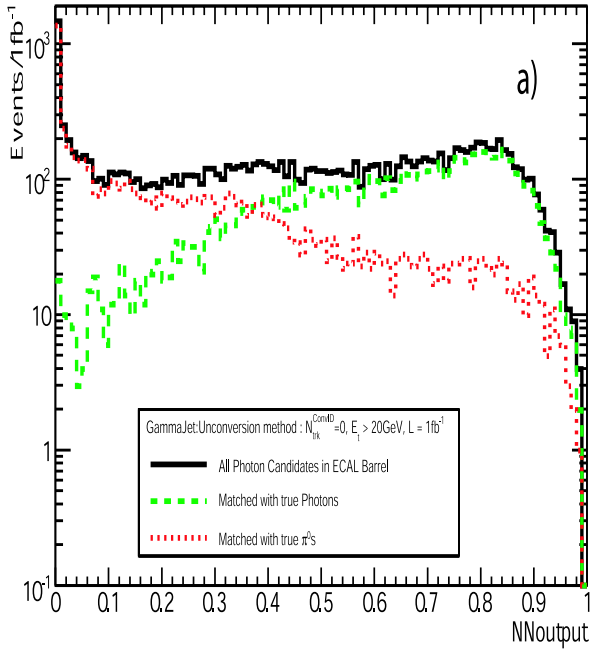
- Select events after applying the HLT2Photon trigger
- apply offline $E_T > 20\text{GeV}$ cut in both photon candidates
- apply isolation to both photon candidates
- select unconverted photon candidates with " $N_{trk}^{ConvID} = 0$ " or " $R9 > 0.93$ " method
- exclude events with $110\text{GeV}/c^2 < M_{\gamma\gamma} < 150\text{GeV}/c^2$ since in this mass region the Higgs signal is supposed to be.
- select a sample enriched in photons putting a cut in higher NNoutput values and a sample enriched in π^0 s putting a cut in lower NNoutput values

As an example we applied the method to "GammaJet" events. In figure 25 the NNoutput is plotted after the above cuts and when " $N_{trk}^{ConvID} = 0$ " method used for selecting unconverted particles. Figure 25 (a) refers to ECAL Barrel region: black solid line all photon candidates, green dashed line candidates matched to real photons, red dot line candidates matched to real π^0 s while 25 refers (c) to the Endcap ECAL ES region with the same color and style notation as in 25 (a). In 25 (b) and (d) the corresponding purity of photons (blue boxes) and π^0 s (red triangles) is calculated from figures 25 (a) and (c) respectively. From these last plots an 80% - 90% pure photon sample can be selected for $0.7 < \text{NNoutput} < 0.9$ while a π^0 sample of the same purity with $\text{NNoutput} < 0.1$. Figure 26 describes the same distributions when " $R9 > 0.93$ " method used for selecting unconverted particles. The distributions 25 (a), (c) and 26 (a), (c) are normalized to $L = 1\text{fb}^{-1}$. Thus, the stability of the ANN to contamination as shown in figure 21, can justify that real data selected with the procedure described above could be used to train the ANN in an iterative procedure.

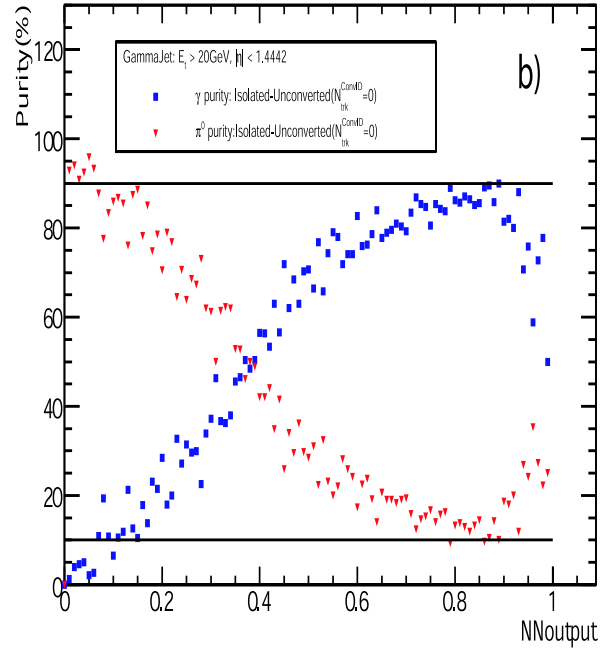
8 Conclusions

In this note we gave an overview of the π^0 rejection algorithm that covers both ECAL Barrel and Endcap ES regions and deals with unconverted particles only. The used method is based in an ANN approach and gave a π^0 rejection for 90% photon efficiency ranging from 29% to 76% depending on the method used for selecting unconverted particles, the E_T and the η range. The application of the algorithm in $H \rightarrow \gamma\gamma$ and $\gamma + Jet$ events simulated without pileups and with 100fb^{-1} misalignment and misscalibration schenario showed that, in case both photon candidates are unconverted, an extra rejection of 46% to 57% for the $\gamma + Jet$ background could be achieved keeping 85% to 88% of the $H \rightarrow \gamma\gamma$ events respectively and this depends on the choise of the unconversion method used. Finally an idea of how to select pure photon or π^0 sample from data was proposed.

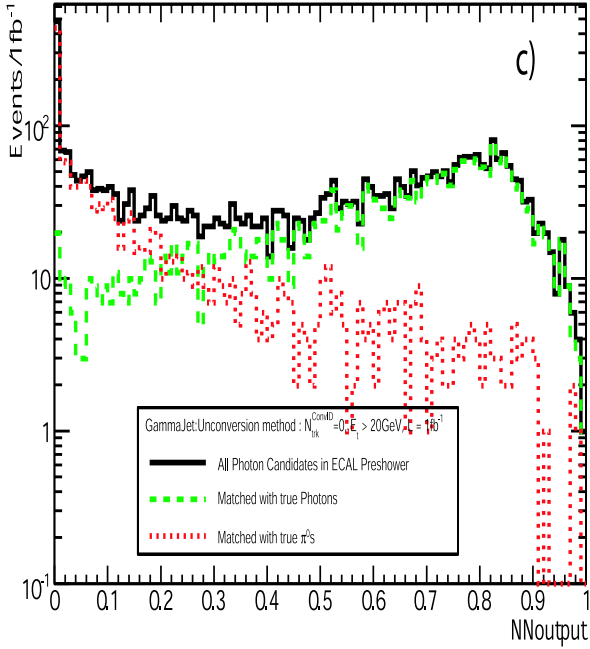
NNOutput from GammaJet events



$\gamma - \pi^0$ Purity



NNOutput from GammaJet events



$\gamma - \pi^0$ Purity

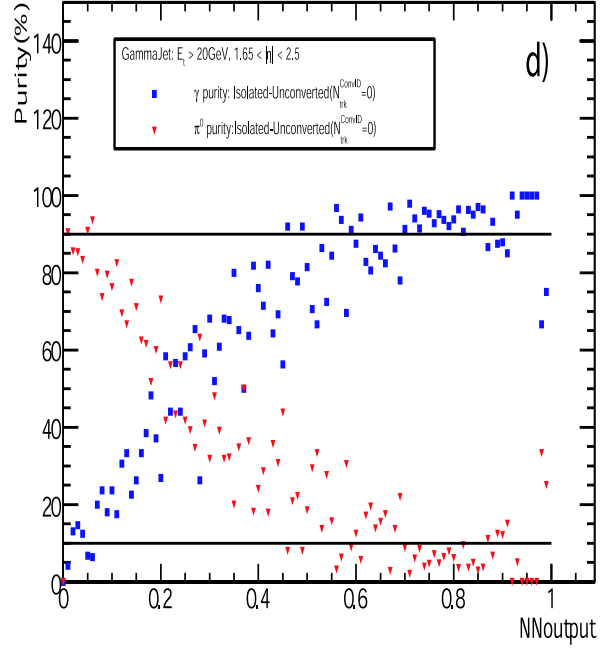
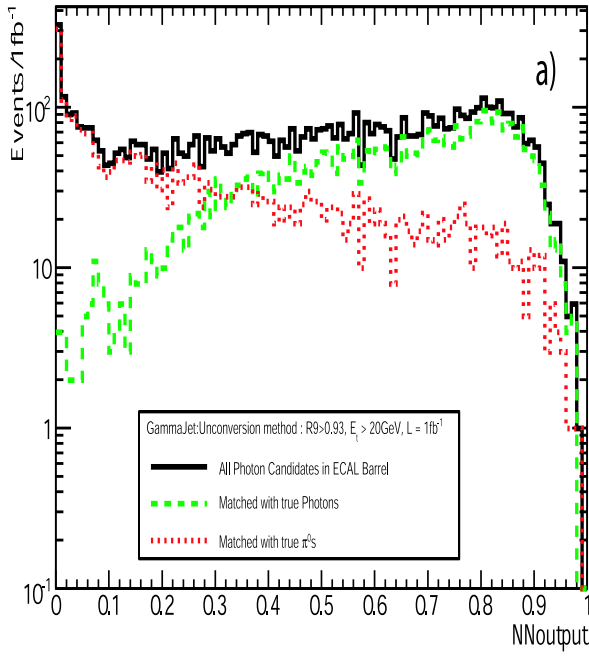
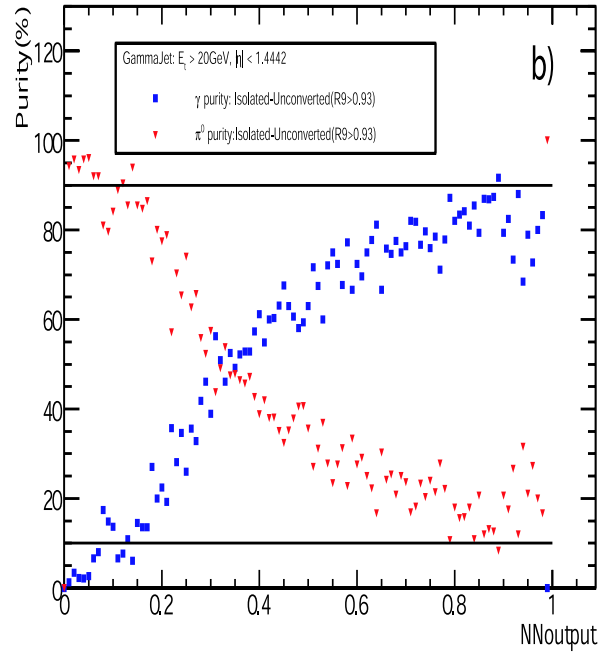


Figure 25: NNOutput of photon candidates from "GammaJet" events after HLT2Photon trigger, offline $E_T > 20\text{GeV}$ cut in both photon candidates, isolation and selection of unconverted particles using " $N_{trk}^{ConvID} = 0$ " method. The photons candidates with $110\text{GeV}/c^2 < M_{\gamma\gamma} < 150\text{GeV}/c^2$ were not taken into account since in this mass region the Higgs signal is supposed to be. (a) ECAL Barrel region: black solid line all photon candidates, green dashed line candidates matched to real photons, red dot line candidates matched to real π^0 s, (b) the purity of photons (blue boxes) and π^0 s (red triangles) calculated from (a), (c) Endcap ECAL ES region: black solid line all photon candidates, green dashed line candidates matched to real photons, red dot line candidates matched to real π^0 s, (d) the purity of photons (blue boxes) and π^0 s (red triangles) calculated from (c). The distributions (a), (c) are normalized to $L = 1\text{fb}^{-1}$

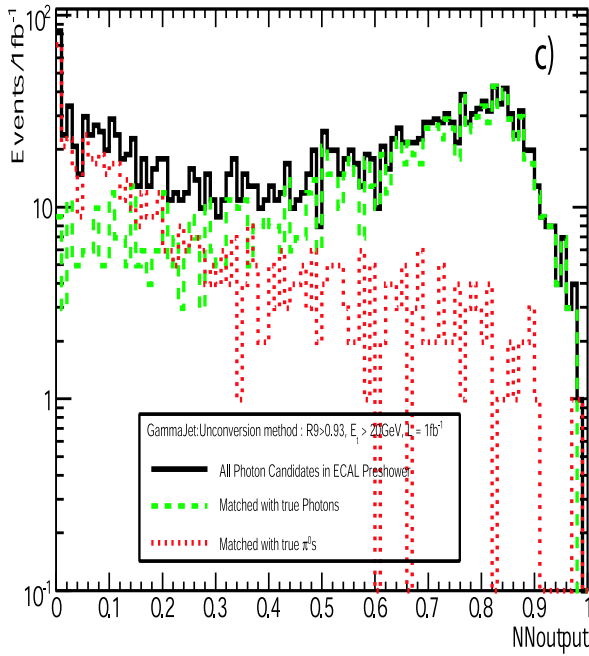
NNOutput from GammaJet events



$\gamma - \pi^0$ Purity



NNOutput from GammaJet events



$\gamma - \pi^0$ Purity

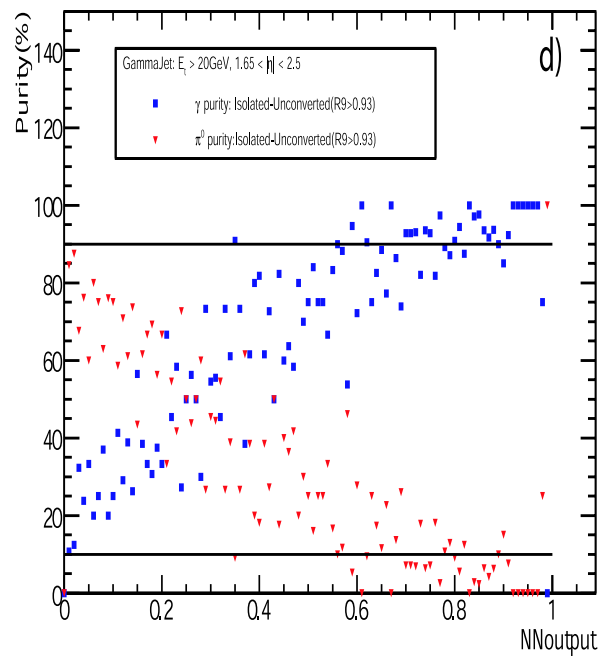


Figure 26: NNOutput of photon candidates from "GammaJet" events after HLT2Photon trigger, offline $E_T > 20\text{GeV}$ cut in both photon candidates, isolation and selection of unconverted particles using "R9 > 0.93" method. The photon candidates with $110\text{GeV}/c^2 < M_{\gamma\gamma} < 150\text{GeV}/c^2$ were not taken into account since in this mass region the Higgs signal is supposed to be. (a) ECAL Barrel region: black solid line all photon candidates, green dashed line candidates matched to real photons, red dot line candidates matched to real π^0 s, (b) the purity of photons (blue boxes) and π^0 s (red triangles) calculated from (a), (c) Endcap ECAL ES region: black solid line all photon candidates, green dashed line candidates matched to real photons, red dot line candidates matched to real π^0 s, (d) the purity of photons (blue boxes) and π^0 s (red triangles) calculated from (c). The distributions (a), (c) are normalized to $L = 1\text{fb}^{-1}$

9 Acknowledgements

We would like to thank Chris Seez, Pascal Vanlaer and David Barney for their suggestions and helpful discussions. This work was carried out with financial support from the Greek General Secretariat for Research and Technology.

References

- [1] “ π^0/γ Discrimination in L3 Using Shower-Shape Analysis”, *D. Kirkby*, **L3 Note 1816**
- [2] CMS TDR 4, **CERN/LHCC 97-33**
- [3] “Neural Networks”, *S. Haykin*
- [4] <https://twiki.cern.ch/twiki/bin/view/CMS/GeneratorProduction2007CSA07Signal>
- [5] “CMS High Level Trigger” *Christos Leonidopoulos et al.*, **CMS AN-2007/009**
- [6] “Inclusive Search for the Higgs Boson in the $H \rightarrow \gamma\gamma$ Channel” *M. Pieri, S. Bhattacharya, I. Fisk, J. Letts, V. Litvin, J.G. Branson*, **CMS-NOTE/06-112**
- [7] “Track finding and identification of converted photons” *N. Marinelli*, **CMS-NOTE/06-005**
- [8] “Jetnet 3.0”, *C. Peterson et al.*, **Comp. Phys. Comm. 88(1994)185**
- [9] “An Artificial Neural Net Approach to Photon - π^0 Discrimination using the CMS Endcap Preshower” *D. Barney, A. Kyriakis, D Loukas, J. Mousa*, **CMS-NOTE/98-088**
- [10] “Neutral pion rejection in the CMS $PbWO_4$ crystal calorimeter using a neural network. The dependence of neutral pion rejection factor on crystal’s off-pointing angle”, *L. Borissov et al.*, **CMS NOTE 1997/050**
- [11] “Electron reconstruction in CMS Electromagnetical Calorimeter” *E. Meschi, T. Monteiro, C. Seez and P. Vikas*, **CMS-NOTE/01-034**
- [12] “TMVA, ToolKit for Multivariate Data Analysis with ROOT” *A.Hocker et al.*, **arXiv physics/0703039**, <http://tmva.sf.net>
- [13] “Neural Pion Rejection at L2 using the CMS Encap Preshower” *D. Barney, A. Kyriakis, D Loukas, J. Mousa, C, Seez*, **CMS-NOTE/99-076**
- [14] “Application of neural networks and ceccular automata to interpretation of calorimeter data”, *V. Breton et al*, **Nuclear Instruments and Methods in Physics Research A362 (1995) 478**